NEUTRON ACTIVATION ANALYSIS OF MANGANESE, IRON AND ZINC IN A RODENT MODEL OF DYSMYELINATION

By

LIANNE R. LOBO, B.Sc.

A Thesis

Submitted to the School of Graduate Studies

In Partial Fulfillment of the Requirements

For the Degree

Master of Science

McMaster University

MASTER OF SCIENCE (2013) McMaster University

Medical Physics & Applied Radiation Sciences Hamilton, Ontario

TITLE: Neutron Activation Analysis of Manganese, Iron and Zinc in a Rodent Model of Dysmyelination

AUTHOR: Lianne R. Lobo,
B.Sc. (Ryerson University)

SUPERVISOR: Dr. Nicholas Bock

NUMBER OF PAGES: x, 49

Abstract

Transition metals have been suggested to play a pivotal role in the pathogenesis of numerous neurological disorders. They serve critical roles in the central nervous system (CNS) as essential cofactors, catalysts, secondary messengers and modulators of genes, enzymes and receptor activity. Manganese (Mn), iron (Fe) and zinc (Zn) are some of the essential metals for normal CNS development and function. Each must be present at specific levels to avoid deficiencies or toxic excess. The research in this thesis investigates the role of transition metals in diseases in which myelin is lost in the central nervous system (CNS). A loss of myelin is termed demyelination, and an example of a disease with prominent demyelination is multiple sclerosis. An incomplete formation of myelin sheaths is termed dysmyelination. This thesis focused on the measurements of manganese, iron and zinc concentrations in a rodent model of dysmyelination; the Long Evans Shaker (*les*) rat.

The Long Evans Shaker (*les*) rat is a fragile, severely dysmyelinated rodent model with body tremors at a young age and severe ataxia in older rats. The mutation causing the severe dysmyelination in these rats is transmitted as an autosomal recessive trait. With a lifespan of 4 to 5 months, the *les* rat is markedly deficient in myelin in the CNS, where most axons are entirely naked and the remaining ones are surrounded by a loosely woven, thin myelin sheath.

In this thesis we studied alterations in manganese, iron and zinc transition metal levels in 3 and 16-week-old *les* rats and their age-matched control counterparts. Using neutron activation analysis (NAA), manganese measurements were made in the brain, spinal cord and visceral organs using an existing protocol, while a new assay was developed for iron and zinc measurements that were made in the spinal cord tissues. The higher trend in manganese concentration observed within the 3 and 16 week old *les* rats in comparison to the controls, where there was a significant increase ($p<0.05$) observed in the 16 week old *les* cerebellum, supports evidence suggesting that manganese levels are associated with astrogliosis. Whereas for iron and zinc, which were measured in the spinal cord tissues, there was also an overall increase in the levels of these metals in the *les* mutant strain when compared to the controls; however, only significant increases in zinc concentration within the 16 week old *les* spinal cords were observed. The overall trend in increased iron in the *les* rats may suggest the oligodendrocyte cells attempt myelination, while the significant increase in zinc that was observed may correlate with extracellular accumulations due to the tremors and seizure episodes often experienced by the *les* rodents.

The characterization of the *les* rodent model mutation and its biochemical abnormality will advance our understanding of not only the process of myelination, but also diseases related to aberrant myelination or the maintenance of myelin sheaths. In particular, the measurements developed in this study may have many applications in demyelinating neurological diseases, where with further optimization, these techniques can be used not only in rodent, but also in human tissue to enhance the understanding of transition metal levels in neurodegenerative diseases.

Acknowledgements

It is a pleasure to thank the many individuals who made this thesis possible. First and foremost, I offer my sincerest gratitude to my supervisor, Dr. Nicholas Bock whose expertise, guidance and patience, added considerably to my graduate work and experience. I would also like to thank my other committee members, Dr. David Chettle and Dr. Andrea Armstrong for all of their valuable assistance and suggestions along the way. I am especially grateful and my sincere thanks go out to Alice Pidrcuzny for all of her help, advice and unsurpassed knowledge of the NAA laboratory techniques that has greatly contributed to my thesis. I would like to also thank Alia Al-Ebraheem for her dedicated time and assistance with the statistical analysis work and to Eyesha Hashim for taking the time to serve as my external reader and "coffee-buddy" over the last two years. I would particularly like to thank my best friend, and the love of my life, Joel Pereira for his help in editing this thesis and for all of his love, humor and encouragement when needed most. Lastly and most importantly, I would like to express my deepest appreciation to my brothers and sisters and in particular, to my parents Luis and Janice Lobo for their unconditional love, support and hard work that they have and continue to put into providing a loving and nurturing environment for my siblings and myself and our ever growing family.

Table of Contents

List of Figures –

List of Tables –

List of Abbreviations –

A – atomic mass

A_o – activity build-up

$A_{standard}$ – peak area of a gamma-ray at a specific energy in the standard

A_{sample} – peak area of a gamma-ray at a specific energy in the sample

A_t – activity after a decay time, t

ATP – adenosine triphosphate

AD – Alzheimer's disease

BBB – blood-brain barrier

BCB – blood-cerebrospinal fluid barrier

CNAA – center for neutron activation analysis

CNS – central nervous system

CP – choroid plexus

Cp – ceruloplasmin

CSF – cerebrospinal fluid

DMT-1 – divalent metal transporter-1

DNA – deoxyribonucleic acid

Fe – iron

Fe^{2+} - divalent iron ion

Fe^{3+} - trivalent iron ion

Fpn – ferroportin

GABA – gamma-aminobutyric acid

GS – glutamine synthetase

HPGe – high purity germanium

le – Long Evans

les – Long Evans Shaker

mbp – myelin basic protein

MCA – multichannel analyzer

md – myelin deficient

Mn – manganese

Mn^{2+} – divalent manganese ion

mPTP – mitochondrial permeability transition pore

MS – multiple sclerosis

MT – metallothionein

n – neutron

NAA – neutron activation analysis

NADPH – nicotinamide adenine dinucleotide phosphate

NIST – National Institute of Standards and Technology

$N_{standard}$ – amount of nuclide present in the standard

N_{sample} – amount of nuclide present in the sample

OLs – oligodendrocytes

OPCs – oligodendrocyte precursor cells

PD – Parkinson's disease

PLP – proteolipid protein

R – count rate

ROS – reactive oxygen species

TfR – transferrin receptor

TfR-ME – transferring receptor-mediated endocytosis

t_i – irradiation time

t_d – decay time

Zn – zinc

Zn^{2+} – divalent zinc ion

γ – gamma photon

ε – absolute detector efficiency

γ – absolute gamma-ray abundance

φ – neutron flux

σ_{th} – thermal neutron capture cross-section

λ – decay constant

Chapter 1 – Introduction

The research in this thesis investigates the role of transition metals in diseases in which myelin is lost in the central nervous system (CNS). Myelin is of fundamental importance to neurons in the CNS. It is an insulating layer made up of proteins and fatty substances that forms around nerve axons, including those in the brain and spinal cord. The purpose of this myelin sheath is to allow impulses to travel quickly and efficiently along axons between nerve cells. If myelin is damaged, the impulses slow down. A loss of myelin is termed demyelination, and an example of a disease with prominent demyelination is multiple sclerosis. An incomplete formation of myelin sheaths is characterized as dysmyelination.

Disruptions in the cellular systems for handling transition metals are observed in neurodegenerative disorders such as Alzheimer's and Parkinson's disease. In many neurodegenerative disorders, both a loss of transition metal homeostasis and myelin breakdown are observed – leading to the question of whether the two are linked.

In an effort to study the roles of transition metals in the complex process of myelination, we studied metal homeostasis in a rodent model with a genetic mutation in its ability to form myelin. The Long Evans Shaker (*les*) rat is a well described CNS myelin mutant with an autosomal recessive mutation in myelin basic protein (*mbp*), which is required for normal myelin development. This mutation almost completely disrupts the development of myelin sheaths in the *les* rat. In this thesis we investigated manganese, iron and zinc transition metal levels in the 3 and 16-week-old *les* rat and the age-matched controls.

My contributions to science through this thesis include:

1. Measuring manganese levels in excised tissues from various brain regions and visceral organs in the *les* model using a neutron activation analysis (NAA) protocol previously developed in our laboratory.

2. Developing and validating an NAA protocol for accurately measuring iron and zinc levels in very small samples of excised rat brain tissue.

3. Using the new protocol to measure iron and zinc levels in spinal cords in the *les* model.

4. Reporting that there are in fact changes in transition metal homeostasis in the *les* model.

This chapter provides a brief background on the biological roles of manganese, iron and zinc in the brain, their homeostatic mechanisms, diseases in which these metals have been implicated and provides a further description of the novel *les* mutant.

1.1 – Essentiality and Function of Transition Metals in the CNS

Transition metal ions have unique biochemical properties that allow them to bind to and be incorporated into proteins. Proteins that bind transition metals are often catalytic enzymes where the transition metal ion is essential for activity. Transition metals such as manganese, iron and zinc are crucial for the proper growth, development, function and maintenance of biological systems.

Manganese is an essential mineral required for normal development and activity in the CNS. It is a trace metal commonly found in the environment. It functions as a cofactor for multiple enzymes, including glutamine synthetase (GS), which participates in the metabolic regulation of the neurotransmitter glutamate in the CNS (Sidoryk-Wegrzynowicz & Aschner, 2013a). Manganese is also found in all body tissues, as it is essential for the synthesis of amino acids, lipids, proteins and carbohydrates (Chen *et al.,* 2006). On the cellular level, manganese is needed for oxidative cellular respiration, reproduction, digestion, and free radical defense. It is a co-factor of several important metalloenzymes that function in the production of ATP via gluconeogenesis, regulation of ammonia levels, and free radical sequestering (Aschner, Erikson & Dorman, 2005). In addition, manganese is a critical cofactor for many key enzymes in the body and is required for proper immune function, regulation of metabolism, reproduction, digestion, bone growth, and blood clotting (Anderson *et al.,* 2008).

Iron is also an essential trace metal required for many biological functions, including oxygen transport, and the proliferation and differentiation of cells via enzymes involved in energy metabolism and DNA synthesis. Iron can cycle between the ferrous (Fe^{2+}) and ferric (Fe^{3+}) states. This ability to accept and donate electrons allows it to serve as an important cofactor for enzymes (Schulz *et al.,* 2011). The importance of iron for normal neurological function has also been well established. Similar to other cells, neurons and glia require iron for many aspects of their physiology, including electron transport, NADPH reductase activity, myelination of axons, and as a cofactor for several enzymes involved in neurotransmitter synthesis (Qian & Wang, 1998). Iron is the most abundant trace metal in the brain and its concentration is region dependent, with ranges in rats starting at 13-24 μg/g at 3 weeks of age and increasing to 24-35 μg/g across various brain regions by 21 weeks of age (Tarohda, Yamamoto & Amamo, 2004). At the cellular level in the central nervous system (CNS), iron levels are the highest in myelin, and in the astrocyte and oligodendrocyte glial cells that support neurons (Connor & Menzies, 1996). In these cells, iron is needed for biosynthetic enzymes involved in lipid and cholesterol synthesis, as well as for enzymes required for the increased metabolic demands of myelination (Hu & Connor, 1996; Schulz *et al.,* 2011).

Another essential trace element, zinc, also plays a key role in many biological processes where it is required for the structural stability of a variety of proteins involved in transcription, protein trafficking and enzyme catalytic activity. Zinc also plays an important physiological role in brain functions involving nucleic acid metabolism, brain tubulin growth and phosphorylation. Studies further demonstrate that zinc is vital to the modulation of synaptic transmission, synaptic plasticity and for the operation of certain

neurotransmitter receptors that are found in high density in the hippocampus brain region (Franklin, Pullen & Hall, 1992; Law *et al.,* 2003; Yanik *et al.,* 2004). In addition to playing a neuromodulator role in regulating diverse populations of neurons and myelinating oligodendrocytes, Zn^{2+}-myelin basic protein and Zn^{2+}-proteolipid protein complexes are reported to be essential for maintaining the integrity of the myelin sheath (Law *et al.,* 2003).

1.2 – Regulation and Codependence of Transition Metals in the CNS

Transition metals must be tightly regulated anywhere in the body due to their strong potential to cause oxidative damage and are therefore always stored and transported by associated chaperone proteins in biological systems. The brain is especially sensitive to toxins; thus, transition metal transport into the CNS is uniquely restricted by the presence of the blood-brain barrier (BBB) that only allows the passage of select molecules and proteins. Transition metals are most often absorbed from the gastrointestinal tract, across the lungs, or through the skin. They then enter systemic circulation. Transition metals may enter the CNS from the blood across the BBB or from the blood by crossing the choroid plexus (CP) into the cerebrospinal fluid (CSF), from which they can diffuse into the CNS.

Transition metals share transport mechanisms because of their similar chemistry and how these pathways operate is important in understanding how transition metal deficiency and over-exposure can occur in the brain (Yokel, 2006). Often it is assumed that transition metals are regulated independently of one another. However, there are recent studies illustrating that transition metals such as iron, zinc and manganese are quite interdependent in the way they are regulated and distributed in the biological system. Thus it is inaccurate to consider individual transition metals in disease in isolation.

Manganese is transported into the CNS across the BBB and the blood-cerebrospinal fluid barrier (BCB), however manganese can also enter the CNS directly following inhalation. It can be transported to the CNS either as a free ion or as a protein-bound species. Cellular manganese transport involves two pathways – the transferrin receptor (TfR) and the divalent metal transporter-1 (DMT-1), with other protein channels implicated as well (Sidoryk-Wegrzynowicz & Aschner, 2013b). More importantly, Mn^{2+} metabolism is high in astrocytes, where glutamine synthetase; an abundantly Mn^{2+}-rich enzyme found exclusively within these cells, catalyzes the conversion of glutamate to glutamine (Aschner, Gannon & Kimelberg, 1992).

Like manganese, iron is capable of catalyzing the production of reactive oxygen species (ROS) and therefore must be also be stringently regulated (Magaki *et al.,* 2007). In the CNS, iron is found in the storage protein ferritin, which is principally expressed in oligodendrocyte and astrocyte glial cell types (Izawa *et al.,* 2010). Iron levels are high in the CNS at birth, and uptake into the brain and spinal cord is a continual process

throughout life. Similar to manganese, iron can enter cells in the CNS via the transferrin receptor (TfR) and through the divalent metal transporter-1 (DMT-1). Small vessels transport iron to the brain via the blood-brain barrier that contains tight junctions that regulate brain iron levels. In addition, fenestrated blood vessels in the choroid plexus, which produces cerebrospinal fluid (CSF), also regulate brain iron (Connor *et al.,* 1992; Hallgren & Sourander, 1958). By controlling the level of expression of the transferrin receptor and ferritin proteins, the cells can determine the amount of iron acquired and sequestered through the BBB (Hu & Connor, 1996). Iron is thought to enter the CNS from the circulation via capillary endothelial cells. As ~ 95% of the capillary surface is covered by astrocytic end feet, astrocytes are ideally positioned to take up iron from the circulation and distribute it to other cells in the CNS (Schulz, Kroner & David, 2012).

Similarly, zinc is essential to the structure and function of numerous proteins and enzymes and so requires tight homeostatic control at both the systemic and cellular level. Zinc is a small, hydrophilic, highly charged species, which cannot cross biological membranes by passive diffusion. However, little information is available regarding the regulation of brain zinc uptake mechanisms (Wang *et al.,* 2011). Zn^{2+} is a key cellular component and its levels in all cells are tightly regulated by the combined actions of transporter proteins, channels and intracellular binding proteins. It is now well recognized that significant amounts of injurious Zn^{2+} can be released from binding sites within postsynaptic neurons, an important constituent of which are the highly abundant metallothionein (MT) proteins. MT proteins contain multiple cysteine residues that can bind up to 7 Zn^{2+} ions, and which can sequester or liberate significant amounts of Zn^{2+} depending on factors such as cellular pH and the redox state of the cell (Shuttleworth & Weiss, 2011). Approximately 10% of total brain Zn^{2+} content is stored within glutamatergic synaptic vesicles (Law *et al.,* 2003).

Due to the chemical and structural similarity amongst transition metals, in organisms ranging from bacteria to mammals, they share and compete for many protein transporters. Dietary or biological environmental changes in one or more of these metals can result in disrupted transport and distribution of transition metals, as well as metal transporter protein expression in the brain and CNS. Therefore in this thesis, we considered the homeostasis of three transition metals in concert.

1.3 – Effects of Deficiency and Overload of Transition Metals in the CNS

Although transition metals have specific biological functions essential for life, lack of regulation of intracellular metal pools can lead to toxicity – often through the formation of oxygen radicals. The resulting reactive oxygen species can go on to damage cellular components including proteins, lipids and nucleic acids, eventually leading to cell death. Perturbations in the balance of transition metals, such as deficiency and overload, are observed in genetic diseases where misregulations manifest in a variety of symptoms and are becoming increasingly implicated in neurodegenerative disorders.

Therefore, complex systems are required to maintain the delicate balance between transition metals as essential nutrients and their potential damaging role as cytotoxins.

Despite the important requirement of manganese for cellular functions, manganese deficiency has only been observed in laboratory animals, since the trace metal is abundant in human diets. Manganese deficiency results in impaired growth, skeletal defects, reduced reproductive function, birth defects, and abnormal lipid and carbohydrate metabolism. However, reduced manganese levels are seen in patients with osteoporosis and epilepsy, where manganese dyshomeostasis is associated with seizure susceptibility (Aschner, Erikson & Dorman, 2005). Likewise, a mounting body of evidence indicates that with a manganese overload, redox-active manganese participates in the pathophysiological processes of numerous disorders of the CNS in humans. Excessive accumulation of manganese in humans results in neurobehavioral deficits such as hyperactivity and manganism. Manganism is characterized by a variety of psychiatric, cognitive and motor disturbances that resemble those inherent to Parkinson's disease (PD). Manganese overload primarily affects the basal ganglia in humans resulting in neuron damage and lesion formation in these gray-matter structures (Canavan, Cobb & Drinker, 1934). The primary exposure route is inhalation, although manganese overload from drinking contaminated well water has also been reported and results in cognitive impairments (Roels *et al.,* 1987; Sahni *et al.,* 2007).

Similar to manganese disorders, iron deficiency impairs cell growth in culture and iron overload can cause cellular damage. Iron deficiency results in malformation of red blood cells, growth impairment, reduced immune function, and deficits in cognition (Beard, Connor & Jones, 1993). However, iron is known to accumulate in the normal aging brain and in greater amounts in several neurologic disorders. In the presence of excess extracellular iron, the iron-carrying capacity of serum transferrin increases. The increased iron-carrying capacity of transferrin and increased rate of iron transportation across the blood-brain barrier results in accumulation of iron in the brain cells (Sadrzadeh & Saffari, 2004). Furthermore, under acidic conditions, iron can be released from ferritin and cause oxidative damage. Abnormally high levels of iron and oxidative stress have been demonstrated in a number of neurodegenerative disorders such as Parkinson's disease and Alzheimer's disease. Such increased levels of brain tissue iron have been implicated as a major generator of reactive oxygen species that are capable of damaging biological molecules (Kozlowski *et al.,* 2009; Quintana & Gutierrez, 2010; Schulz *et al.,* 2011). Interestingly, some genetic iron metabolism disorders, such as hematochromatosis, do not necessarily result in iron overload in the CNS, thus highlighting the central nervous system's ability to maintain homeostasis in the presence of systemic overload. Nevertheless, it is still not clear whether iron accumulation is the initial cause or a secondary consequence of diseases (Quintana & Gutierrez, 2010).

Finally, studies also show that dietary zinc deficiency leads to changes in the central nervous system resulting in behavioral abnormalities. Zinc deficiency also increases glutamate release and thus pathological processes associated with glutamate excitotoxicity are associated with zinc deficiency (Omata *et al.,* 2012). However excess zinc, which is released in the synaptic clefts, causes the apoptotic death of the target

neurons (Wang *et al.,* 2011). Recent work on animal models and human subjects raises the possibility that a significant contributor to Zn^{2+} release and accumulation could be repetitive spreading depolarizations that occur in the hours and days after stroke. Moreover, Zn^{2+} influx from the extracellular space is well demonstrated to induce injury in cultured neurons, often after entry through channels and transporters that were originally defined as Ca^{2+}-permeable. Oxidative stress and acidosis (both of which occur prominently in ischemia) can induce Zn^{2+} release from metallothionein (MT) proteins, resulting in substantial increases in intracellular Zn^{2+}. It is also possible that the efflux of Zn^{2+} from mitochondria could contribute directly to cytosolic Zn^{2+} increases through pathways that include depolarization and opening of the mitochondrial permeability transition pore (mPTP). Pathological Zn^{2+} accumulation can affect mitochondrial function in various ways. Zn^{2+} induces swelling and the release of reactive oxygen species (ROS) from mitochondria in isolation or in cultured neurons. Toxic intracellular Zn^{2+} accumulation can lead to prominent metabolic consequences. Importantly, these events may be amplified because Zn^{2+}-triggered ROS generation can trigger further intracellular Zn^{2+} mobilization (Shuttleworth & Weiss, 2011).

1.4 – Transition Metals and Diseases Involving Myelin

Given the evidence for the involvement of transition metals in many brain diseases, one can question whether they are involved in diseases where myelination is disrupted.

The central nervous system (CNS) is primarily composed of two broad classes of cells: neurons and glial cells. Astrocytes are a class of glial cells in the CNS that are responsible for holding neurons in place, providing them with nutrients and digesting parts of dead neurons. In addition, astrocytes can communicate with neurons and modify the signals they send or receive (University of Utah, 2013). Recent evidence suggests that astrocytes may play a key role in regulating demyelinating CNS diseases. In particular, reactive astrogliosis is a prominent feature in inflammatory CNS conditions that occur in multiple sclerosis and experimental autoimmune encephalomyelitis (EAE); an inflammation-driven animal model of CNS demyelination. The role of astrocytes in demyelinating diseases is controversial, and both protective as well as deleterious effects on demyelination are being discussed (De Keyser *et al.,* 2010; Moore *et al.,* 2011; Williams, Piaton & Lubetzki, 2007). Astrocytes are suggested to exert detrimental effects and promote demyelination by enhancing the immune response through expression of cytokines and recruitment of T cells, microglia and macrophages to demyelinating lesions. In contrast, favorable effects of astrocytes on demyelination have also been proposed. The formation of a glial scar is supposed to be a physical barrier against inflammatory cells entering demyelinated areas (Skripuletz *et al.,* 2013).

In chronic degenerative or demyelinating diseases of the CNS, reactive microglia are found to be associated with senile plaques in Alzheimer's disease or demyelinated axons in diseases such as multiple sclerosis. The roles of activated microglia in these

disease processes remain unclear (Zhang *et al.,* 2001). However, numerous studies have observed that manganese has been implicated in the pathophysiology of several neurodegenerative diseases. Excess deposition of manganese in the CNS leads to neurological abnormalities such as manganism, which is associated with hypokinesia, rigidity and tremor; symptoms that resemble those of Parkinson's disease. Manganese in the brain is preferentially deposited in astrocytes because of the presence of high capacity transporters in these cells. Such preferential accumulation suggests that astrocytes may be more vulnerable to manganese toxicity than other neural cells. While mechanisms of manganese neurotoxicity are not completely understood, oxidative stress has been implicated in its toxicity (Erikson *et al.,* 2004). Evidence shows that manganese exposure results in cell swelling in cultured astrocytes. Such swelling appears to be, at least in part, a consequence of oxidative stress (Rama Rao *et al.,* 2007). Therefore, astrocyte swelling may represent an important pathological event associated with manganese toxicity, contributing to the pathogenesis of manganism and numerous other neurodegenerative diseases (Rama Rao *et al.,* 2007).

The formation of myelin in the central nervous system is crucial to proper development and function. Oligodendrocytes are glial cells in the CNS that are responsible for the formation of myelin that insulate neurons. A single oligodendrocyte cell may ensheath up to 60 separate axons (Miller, 2002). Myelinated axons form the white matter in the brain that serves as a communication link between different brain regions. White matter abnormalities result in cognitive deficits as is observed in several neurodegenerative disorders, including the autoimmune disease multiple sclerosis.

An autoimmune disease is characterized by the loss of self-tolerance of the immune system, which can be caused by either genetic or environmental factors or a combination of both. As a consequence of this malfunction, an immune response is initiated against certain cell types or even entire organs of the body. For the central nervous system (CNS), several autoimmune diseases are described of which multiple sclerosis (MS) is the most common form. MS comprises of a blood-brain-barrier (BBB) disruption accompanied by an activation of macrophages/microglia within the CNS, ultimately resulting in demyelination and degeneration of neuronal structures. The activation of microglia has been described in the damaged CNS during the pathology of MS, reflecting an initial event in MS pathology. In early stages of MS, reactive microglia clusters are found in lesions in the white matter of MS patients (Goldmann & Prinz, 2013). Such similar CNS autoimmune characteristics are also observed in the Long Evans Shaker (*les*) rodent model. In this study, the *les* rat brain tissue regions and spinal cord tissue samples were investigated to elucidate the roles of manganese, iron and zinc metal levels in such myelin-related neurodegenerative diseases.

1.5 – The Dysmyelinated Long Evans Shaker Rat Model

As mentioned in the introduction, the focus of this thesis is the role of transition metals in diseases involving disruptions in myelination. Rodent models for the study of

demyelination have been extensively explored to gain a better understanding of these disease states. In particular, our lab has previously focused on models of demyelination such as the cuprizone study, where successful transition metal measurements were made in an effort to elucidate their effects in neurodegenerative diseases (Moldovan, 2012). However, in this research, a novel rat model of dysmyelination is investigated. Specifically, whereas demyelination consists of autoimmune diseases resulting in the loss of myelin sheaths at some later time, dysmyelination is characterized by the immediate defect in structure and function of myelin sheaths that often arises from genetic mutations that affect the biosynthesis and formation of myelin. This thesis investigates potential alterations in transition metal levels in this model.

Generally, the rat CNS, including the myelination of axons, develops in a caudocranial sequential manner and is considered mature by 2 months of age. The myelination process progresses rapidly in the nervous system of the rat, where the ventral nervous system is myelinated by 48 h, cranial nerves by 7 days, and the medulla, pons, and midbrain by 21 days of age (Delaney *et al.,* 1995). Numerous rodent models of inherited disorders of myelination have been described in order to study the structure of myelin, its components, and the complex process of myelination. The Long Evans Shaker (*les*) rat is an autosomal recessive mutant model of dysmyelination. In a pattern similar to that of most other myelin mutants, the *les* rat has a phenotype characterized by tremor, seizure, and early death. Distinguished full-body tremors by 10 to 14 days of age initially characterize the *les* rat, such that bouncing and shaking movements of the trunk depict the tremors. With age, the tremors decrease in amplitude and eventually become a rocking motion when a *les* rat attempts to ambulate. Seizures begin in these rats from 5 to 14 weeks of age, at a frequency of 4 to 5 times daily. Individual seizures last 30 to 45 seconds where the animal is laterally recumbent with marked extensor rigidity that is then followed by a 45 to 60 second period of disorientation and lethargy (Delaney *et al.,* 1995). Initially, stimuli such as loud noises or movement of the cage initiate the seizures, however with age, seizures are initiated without a stimulus. Progressive ataxia, hind limb paresis, and eventual paralysis have been observed in the affected rats (Delaney *et al.,* 1995).

The *les* rat is distinguished for having very little myelin in the CNS, where most of its axons are not myelinated, yet has the ability to survive up to 4 or 5 months. In this thesis, transition metal levels were studied in the dysmyelinated rodent model; the Long Evans Shaker rat (*les)* and in its control counterpart, the Long Evans rat (*le*). The two age groups under study were the three-week and sixteen-week old control and Shaker rats. Using two independent neutron activation analysis assays, manganese concentration measurements were made in the visceral organs, spinal cords and the five distinguished regions of the brain, while iron and zinc concentrations were studied in the control and Shaker rat spinal cords.

Chapter 2 – Metal Measurements with Neutron Activation Analysis

2.1 – Neutron Activation Analysis

In this research, we used neutron activation analysis (NAA) to measure manganese in the tissue samples, and investigated its use for measuring iron and zinc concentrations. Unlike NAA, other methods that provide a means of measuring metal concentrations are hindered by the necessary chemical preparation of samples, which can lead to sample contamination and variability in the measurements. Alternatively, NAA is a nondestructive technique with detection sensitivity for manganese of less than 1 μg; thus making it a sensitive analytical process for performing both qualitative and quantitative multi-element analysis of major, minor and trace elements (Pidruczny *et al.,* 1994).

In this chapter, it is important to note that the considerations of the NAA assay vary depending on the target isotope. In particular, NAA is far more sensitive for measuring manganese than it is for measuring iron and zinc. This results from the relatively smaller cross-sections of 0.726 barns for zinc and 1.31 barns for iron, in comparison to the larger cross section of 13.2 barns for manganese. In addition, the long half-lives of 44.5 days and 243.9 days for iron and zinc respectively also contribute to a low yield of activated daughter product. Therefore, the irradiation protocols for NAA of iron and zinc developed in this thesis had a much lower throughput than the manganese protocol.

2.1.1 – Principles of Neutron Activation Analysis

Neutron activation analysis is a nuclear excitation process based on the inelastic interaction of neutrons with a target nucleus. Samples with unknown elemental concentrations are irradiated with neutrons, together with standard materials with known elemental concentrations. When neutrons are absorbed in the nuclei of constituent atoms the stable nuclides undergo neutron capture reactions to produce radionuclides. The neutron capture reaction is given by

$$^{A}Z\,(n,\gamma)\,^{A+1}Z \qquad (1)$$

where n is a neutron, γ is a gamma photon, and A is the atomic mass.

The radioactive nuclides activated in a sample will have a unique half-life, mode of decay and energy of emitted gamma radiations during its decay. The emitted gamma rays are unique for each isotope and the amount of gamma radiation given off at certain energies are indicative of the amount of the element present in the sample. Comparing the specific

activities induced in the standards and unknowns provides the basis for computation of elemental abundances (Glascock, 1988). Therefore, using a comparative method in this study, standards and samples were simultaneously exposed to the neutron flux in the McMaster Nuclear Reactor. Following irradiation, the standards and samples were measured under the same conditions using nuclear spectroscopy techniques. This relative approach simplifies data analysis as it reduces the experimental parameters that must be accounted for and is the technique used in this research.

2.1.2 – Irradiation facilities

Nuclear reactors are the most efficient neutron sources for elemental analysis due to the high neutron flux. Neutrons in the thermal energy range around 0.025eV are typically chosen since the majority of elements have a high neutron capture cross-section, which gives a measure of the probability of neutron capture, in the thermal region (Mughabghab, 2003).

All NAA samples in this study were irradiated in the reactor core at the McMaster Nuclear Reactor (MNR). The MNR is a thermal, 5 MW open pool research reactor facility that utilizes plate-type Low Enriched Uranium (LEU, <20% ^{235}U) fuel and is moderated and cooled with light water (McMaster University, 1996-2013). The moderately high neutron fluxes available in or near the reactor core make the MNR invaluable for sensitive NAA. For the study of manganese, a system (called RABBIT) was used to irradiate the tissue samples. This system consists of 5 irradiation terminals that are adjacent to the core and that are accessed by an automatic, computer controlled pneumatic transport system. The samples are loaded in the RABBIT pneumatic sample transfer system in the Center for Neutron Activation Analysis (CNAA) – an on-site laboratory equipped for NAA elemental analysis. Through this lab, the samples are delivered to and retrieved from the reactor core via the pneumatic vacuum system. The thermal flux at these sites of irradiation is approximately 10^{12} n/cm^2 s (Pidruczny *et al.*, 1994). This serves as an efficient method for short irradiations, while simultaneously exposing the samples to a high neutron flux. On the other hand, for longer irradiations; such as was required for the measurement of iron and zinc, samples were delivered to the reactor where they were situated near the reactor core for a two week period of irradiation. The site of NAA used for these irradiations was 2A. This site is exposed to a thermal neutron flux of an order of magnitude of 10^{13} n/cm^2 s (Pidruczny *et al.*, 1994). Table 1 below describes the flux ranges for the various sites that are illustrated in Figure 1.

Table 1: Description of irradiation facilities (Pidruczny *et al.*, 1994).

Site	Size [mm] L	D	No. of sites	Flux [n/cm^{2}s]
CAPSULES	40	18	9	4×10^{13}
RIFLS*	750	60	2	5×10^{12}
LVR*	750	125	1	3×10^{11}
DRY TUBES	750	60	1	1×10^{12}
RABBITS	50	13	5	3×10^{12}

*RIFLS – Reactor Irradiation Facility for Large Samples
*LVR – Large Volume RIFLS

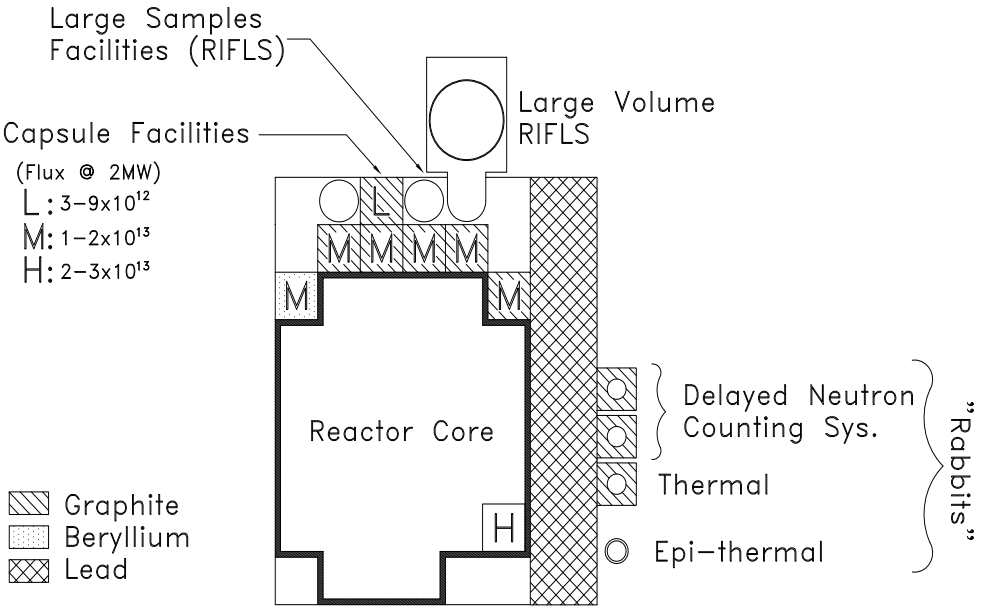

Figure 1: Location of irradiation sites at the McMaster Nuclear Reactor (Pidruczny *et al.*, 1994).

2.2 – Gamma Spectroscopy and the HPGe Detector

With NAA, multi-elemental analysis is feasible by the use of a high-resolution, high purity germanium (HPGe) semiconductor detector to identify and measure the emitted gamma ray spectrum (Glascock, 1988). HPGe detectors consist of a high purity germanium material with an impurity concentration of 10^{10} atoms/cm^3; a PC based

multichannel analyzer (MCA); associated electronics such as a preamplifier, high voltage filter, shaping amplifier; and software for data analysis (Knoll, 2000).

HPGe detectors are used in gamma spectroscopy due to their exceptional energy resolution. When exposed to ionizing radiation, the detector directly collects the charges produced by the ionization of the semiconductor material. On average, one electron-hole pair is produced for approximately every 3 eV absorbed from the radiation. These pairs drift under an external electric field to the electrodes where the pulse is generated. By creating a p-n junction at one electrode and polarizing it so that no current passes through when there is no ionizing radiation, creates a region called the depletion layer. This is where few charge carriers remain, thus resembling a pure semiconductor. With a sufficient voltage, the electric field can create a large enough depleted volume region that is sensitive to ionizing X-ray and γ-ray radiations. Furthermore, in order to reduce electronic noise from a leakage current, HPGe detectors must be cooled to liquid nitrogen temperatures due to the small band-gap energy of germanium. The germanium crystal is encased in a cryostat under high vacuum with the preamplifier (Knoll, 2000). Thus the major characteristics of the HPGe detector are its high atomic number relative to other detectors, low impurity concentration (large depletion depth), low ionizing radiation energy required to produce an electron-hole pair, high conductivity, high resolution and relative simplicity of operation.

The HPGe detector used in this research is an n-type high-purity germanium coaxial closed-ended semiconductor crystal. It consists of an n-type cylindrical germanium crystal with the p^+ electrode at its outer surface and the n^+ electrode located at the inner surface of the central hole forming a p-n junction at the outer surface of the crystal. The depletion region is increased by reverse biasing the p-n junction. The electric field within the region of the junction allows for collection of the electron-hole pairs generated within the depletion region by interaction with gamma photons emitted by the radionuclides in the activated sample. The motion of electrons and holes drifting toward the collecting electrodes creates an electrical signal proportional to the initial deposited energy by the photon (Knoll, 2000).

Gamma ray detection is based on the energy deposition of gamma rays interacting with matter. The three important types of interaction of a γ-ray with matter include the photoelectric effect, the Compton effect and pair-production. The photoelectric effect is significant for the incident gamma energies of 0-150 keV. For γ-ray energies greater than 150 keV and less than 8.5 MeV, the Compton effect contributes strongly to the full energy peak. Compton scattering also contributes strongly to the full energy peak by multiple Compton scattering under the condition that the last interaction is a photoelectric one and that all the preceding Compton interactions take place in the germanium crystal. A pulse will contribute to the Compton continuum if the last interaction does not occur by the photoelectric effect or if one of the multiple Compton interactions takes place outside of the volume of the detector. Pair production also contributes to the gamma ray spectra for γ-ray energies greater than 1.02 MeV. From the law of conservation of mass and energy, it follows that the initial gamma ray must have an energy of 1.02 MeV or greater since that is the energy required to produce the electron-positron pair. When this

amount of energy is deposited, a pair production interaction may occur within the detector (Khandaker, 2011).

Once the electrical signal is produced by the interaction of the γ-rays with the detector material, it is processed in the preamplifier, in the high voltage filter and by the shaping amplifier to produce a filtered, shaped and amplified signal pulse. The multichannel analyzer (MCA) sorts the signals and displays the pulse height distribution in a histogram that exhibits the number of events versus the pulse height that relates to the energy spectrum of the gamma rays collected (ORTEC, 2010). Following an energy calibration, a spectrum of counts versus energy is displayed by the PC based MCA. The measured count of gamma rays of a specific energy depends on the quantity of the element in the biological sample. The count rate, R, of the detected gamma photons emitted by a radionuclide is related to the amount of the nuclide activated in the sample, N_{sample}, by the following expression

$$R = \varepsilon\, \gamma\, N_{sample}\, \varphi\, \sigma\, (1 - e^{-\lambda t_i}) e^{-\lambda t_d} \qquad (2)$$

where ε is the absolute detector efficiency, γ is the absolute gamma-ray abundance, φ is the neutron flux, σ is the neutron capture cross-section, λ is the decay constant, t_i is the irradiation time, and t_d is the decay time (University of Missouri, 2008).

In practice, it is difficult to establish all of the above parameters and the comparative, instrumental NAA method is therefore used in this work. When standards are irradiated and measured using the same protocol as the samples, then the quantities of the nuclide sought out in the samples are related by

$$\frac{N_{sample}}{N_{standard}} = \frac{A_{sample}}{A_{standard}} \qquad (3)$$

where A_{sample} and $A_{standard}$ are the peak areas of a gamma ray of a specific energy in the sample and standard measurements respectively, and where $N_{standard}$ is the amount of nuclide activated in the standard. This then allows for easy and efficient determination of the amount of nuclide present in the sample (N_{sample}) (Glascock, 1988).

2.3 – Manganese Neutron Activation Analysis

A previous Masters' student in our laboratory developed the comparative neutron activation analysis technique that was used to measure manganese in this study. This protocol, as described below, was used to measure the manganese content in the five brain regions of interest, the spinal cord tissues and in the visceral organs.

Standards of 1μg manganese were made up from a 1000 μg/mL manganese standard stock solution (J.T. Baker 6458-04, NJ). The manganese standards and the rat

tissue samples were irradiated for 1200 seconds using the RABBIT thermalized neutron irradiation site at the McMaster Nuclear Reactor. After a 4500 second delay time, the irradiated samples were measured using an Aptec HPGe spectroscopy system with a counting time of 900 seconds. The HPGe detector is an Ortec model GMX-25195-S detector biased at 3kV with a 0.5 mm beryllium window. The detector is cooled by a 16L liquid nitrogen dewar in the Ortec CFG-SH-GMX configuration. The PC based MCA is an Aptec PCMCA/WIN v4.3 Release 6 system configured to 16384 channels.

During the time of irradiations, the manganese standards were measured as the first and last samples and were averaged to account for any temporal changes in flux. The photopeak associated with the 847 keV gamma ray decay of Mn-56 was chosen for analysis since it has the highest emission probability. The ratio of the sample to the average standard peak areas was used to calculate the mass of manganese in the tissue samples. The peak areas were determined using the Aptec software for the standards and tissue samples. The manganese concentrations in the 5 brain regions, spinal cord, kidney and liver samples were then obtained by dividing the mass of manganese in the sample by the wet weight of the sample in order to get the μg/g weight.

Using the United States' National Institute of Standards and Technology (NIST) certified bovine muscle powder standard reference material (Reference Material 8414), the accuracy for the manganese comparative NAA technique was validated. The bovine muscle tissue sample sizes were chosen so as to simulate the average freeze-dried regional brain region weights to determine whether trace amounts of manganese would be measurable. The certified and experimentally observed concentrations of manganese in the bovine muscle reference material are given below in Table 2, and are in good agreement with one another.

Table 2: Certified and experimental concentrations of Mn in the NIST bovine muscle powder standard

Element	NIST Certified Mn Concentration [μg/g]	Experimental Mn Concentration [μg/g]
Manganese (Mn)	0.37 ± 0.09	0.39 ± 0.09

Table 2 illustrates that this NAA method is accurate for the measurements of manganese in small biological, rodent tissue samples. The errors associated with the reported values in Table 2 are as follows – NIST: mean ± uncertainty weight and experimental concentration: mean ± standard deviation (n=5). The standard deviations from the measurements in this study originate from the average taken across a number of sample measurements.

2.4 – Iron and Zinc Neutron Activation Analysis

To measure the iron and zinc contents in the spinal cord tissue samples, a similar comparative neutron activation analysis based technique was developed and optimized to efficiently measure these elements as described below.

2.4.1 – Simulation Data

Traditional chemical analysis methods have provided evidence for a contributory role of iron and zinc in the pathogenesis of certain neurological diseases. However, the measurements for these studies have been based on methods that have limited reproducibility, especially when considering very small rodent brain tissue samples. An alternative way of studying iron and zinc in *ex vivo* tissue samples is neutron activation analysis (NAA).

Iron and zinc isotopes that are suitable for NAA are ^{58}Fe and ^{64}Zn. When exposed to a neutron field, iron and zinc activate primarily through the corresponding capture reactions ^{58}Fe (n,γ) ^{59}Fe and ^{64}Zn (n,γ) ^{65}Zn. The daughter products, ^{59}Fe and ^{65}Zn decay with respective half-lives of 44.5 days and 243.9 days to ^{59}Co and ^{65}Cu respectively. The gamma rays emitted during the decay of the ^{59}Fe and ^{65}Zn nuclei have dominating energies with a corresponding percent abundance of 1099.25 keV at 56.5% and 1115.55 keV at 50.7%. The inactive isotopes of iron and zinc have activation thermal cross-sections of 1.31 barns and 0.726 barns respectively (Glascock, 1988). This illustrates that these isotopes have an appropriate efficiency of irradiation. Specifically, there is an effective neutron absorption cross-section for thermal neutrons that allows for easy absorption by the atomic nucleus. In addition, since the iron and zinc nuclides obtained also have long half-lives, this contributes to a low yield that must be compensated by a long irradiation time in a high neutron flux to effectively measure iron and zinc in the small aliquots of the tissue samples (Johansson *et al.,* 1970).

To determine the appropriate NAA method to efficiently measure iron and zinc in biological samples, a MATLAB code was written. This was to simulate and determine the optimum irradiation time to effectively activate the iron and zinc present in the tissue sample while also defining an ideal decay time prior to measurements. In particular, other elements within the tissue samples that are activated and produce their own signals may interfere with and limit the measurement of the iron and zinc gamma lines. Therefore, to avoid limitations of the major sources of interfering signals, a sufficient decay time must also be decided upon. Hence, to simulate the optimal irradiation technique and procedure, modeling of isotopic activity build-up and decay curves are a useful tool to determine which experimental conditions will yield maximum iron and zinc signals without significant interference.

The major elements present in biological tissues that produce a competing signal for the iron and zinc gamma peaks are those with a gamma energy close to 1099 keV and 1115 keV and those with a higher gamma energy which contribute to the underlying

Compton plateau. The potentially interfering radioisotopes in biological tissue samples that were considered when developing the iron and zinc NAA technique were sodium (^{24}Na) and potassium (^{42}K). The table below lists the respective elemental abundances, half-lives and gamma energies for the elements of interest in this study.

Table 3: Half-lives and gamma-ray energies for elemental spectra

Element	Parent Isotopic abundance [%]	Reaction	Cross-section [b]	Half-life	Gamma Energy [keV]	Decay Product
^{23}Na	1	^{23}Na(n,γ)^{24}Na	0.513	14.96 h	1368.60	^{24}Mg
^{41}K	0.0673	^{41}K(n,γ)^{42}K	1.45	12.36 h	1524.58	^{42}Ca
^{55}Mn	100	^{55}Mn(n,γ)^{56}Mn	13.2	2.58 h	846.76	^{56}Fe
^{58}Fe	0.28	^{58}Fe(n,γ)^{59}Fe	1.31	44.5 d	1099.25	^{59}Co
^{64}Zn	48.6	^{64}Zn(n,γ)^{65}Zn	0.726	243.9 d	1115.55	^{65}Cu

The equation used to determine the activity build up in the simulation was as follows:

$$A_o = N\,\sigma_{th}\,\varphi\,(1 - e^{-\lambda t_{irr}}) \qquad (4)$$

where A_o is the activity produced for the radionuclide of interest, N is the number of target atoms in the sample, σ_{th} is the thermal cross-section for the reaction that produces the radionuclide, φ is the neutron flux, λ is the decay constant and t_{irr} is the irradiation time (Glascock, 1988). After irradiation, the number of radioactive atoms decreases according to the unique half-life of the radionuclide. The equation used to represent this process is described by the expression:

$$A_t = A_o\,e^{-\lambda t_d} \qquad (5)$$

where A_t is the radioactivity of the isotope after the decay time, t_d, following irradiation (Glascock, 1988). Note that the number of target atoms for N was calculated by using a weighted value of the United States' National Institute of Standards and Technology (NIST) certified bovine muscle tissue powder that would simulate the weight of an average brain sample. This was to verify that iron and zinc could be measured in very small biological samples using this NAA assay.

Overall, the rate of activity build-up is linearly dependent on the product of the parent isotope abundance and the cross-section for the reaction and non-linearly dependent on the half-life of the daughter product. Therefore, it was concluded that a long irradiation time would be best suited to saturate the activity build-up of sodium, and potassium in the measurement protocol, since these elements have fairly short half-lives

in comparison to iron and zinc. Once these elements reach a saturated level of activation, further irradiation would thereafter maximize the relative activation of the iron and zinc isotopes within the tissue samples. More specifically, the element producing interference that is slowest to saturate is sodium, which has a half-life of roughly 15 hours (see Table 3). Once sodium reaches its maximal activity build-up after approximately 5 days, any further irradiation preferentially increases builds up towards the activity saturation of iron and zinc. However, using a simulated MATLAB code, the model in Figure 2 below illustrates that it is not practical to continue irradiating to the point of iron and zinc saturation since this would require over a year to saturate iron alone.

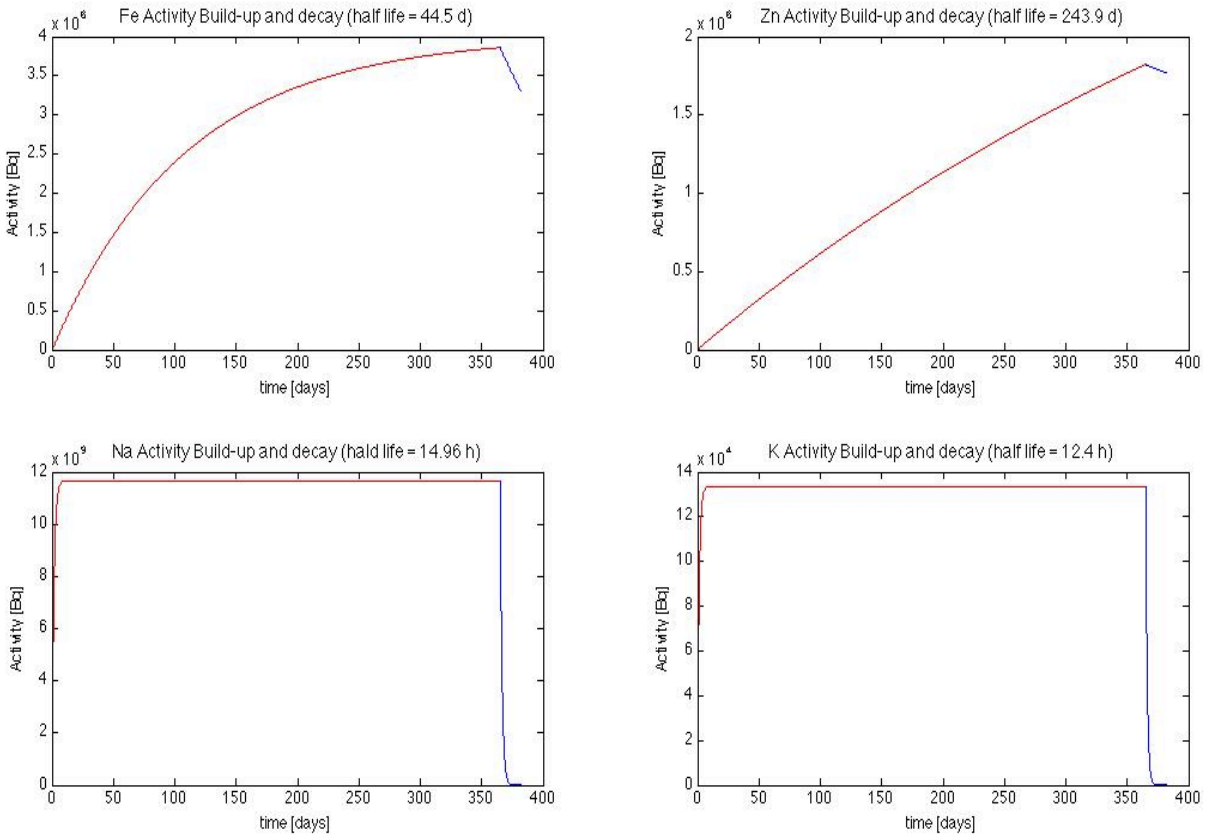

Figure 2: Simulation data of activity build-up (shown in red) and decay (shown in blue) of iron, zinc, sodium and potassium following a 365 day irradiation period in the reactor core to reach activity saturation of iron.

Hence, after modeling the activity build up and considering sample throughput logistics, it was decided that an irradiation time of 10 days would be most practical and allowable since the reactor is also a shared site for other researchers and industrial work. Below in Figure 3, the activity build-up and decay of Fe, Zn, Na and K from the MATLAB simulation are illustrated for the most practical throughput for the analysis of

iron and zinc. The red lines indicate the activity build-up after the decided 10 day irradiation period, whereas the blue lines model the decay of the nuclides following irradiation. The graphs illustrate that the most ideal time at which a sample count can be taken to efficiently detect the signal from iron and zinc would be when sodium, which produces the largest signal interference, decays to an acceptable amount. In addition, due to radioactivity regulations at the McMaster Nuclear Reactor, the samples are too radioactive for handling prior to this time. Therefore, with all of these considerations, the effective delay corresponds to a time period of approximately 10 days following the end of the irradiation time. At this point, the activity from sodium and potassium are reduced to 0.002% and virtually 0% respectively of their original values, whereas the counts from iron and zinc are only reduced to 85.6% and 97.2% respectively.

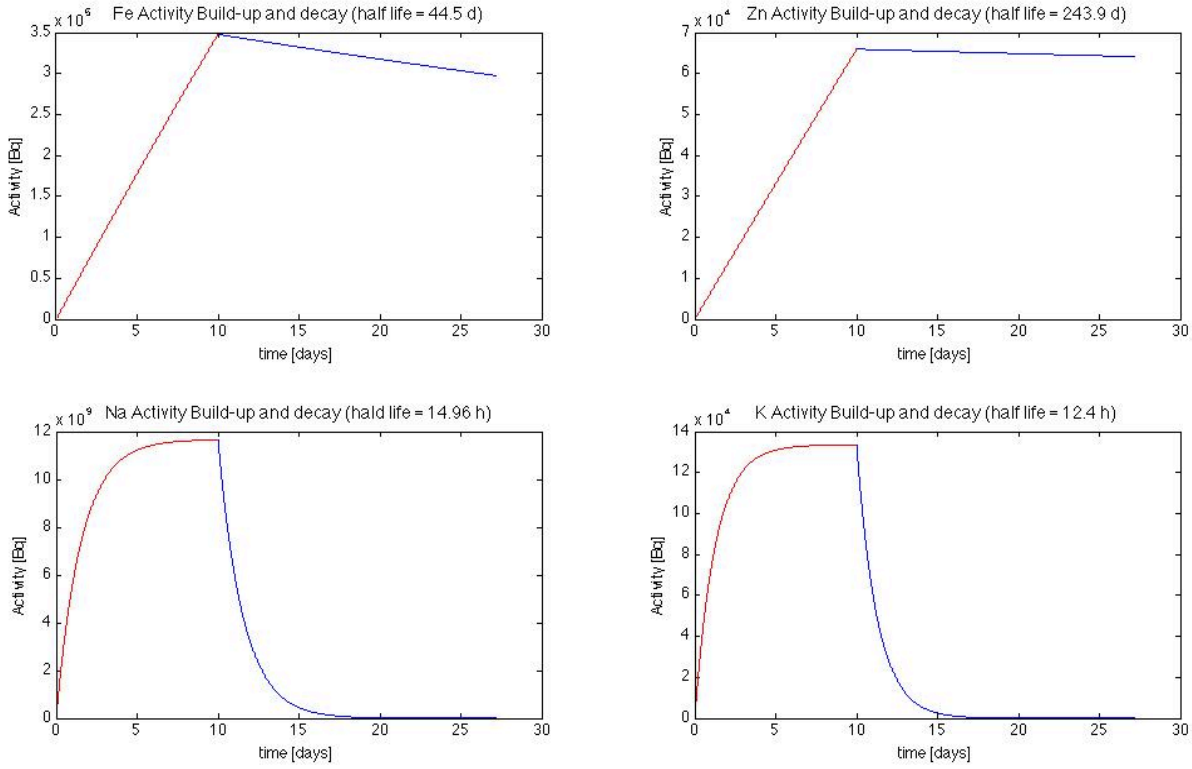

Figure 3: Simulation data of optimal activity build-up (shown in red) during a 10 day irradiation period followed by a 10 day decay time (shown in blue) of iron, zinc, sodium and potassium.

2.4.2 – Flux Measurements

Knowledge of the thermal neutron flux, the time integral over flux density, is necessary for the evaluation of many reactor experiments. It is especially important in comparative NAA that the flux at the samples and standards is the same. The flux received by the experimental assembly is normally determined by using a monitor

installed in or near the assembly during the entire irradiation period. Any experiment done with reactors requires knowledge of the integrated neutron flux.

In this study, eight quartz tubes, including two standards, with one in the top and the other in the bottom row, were placed in a single aluminum canister for irradiation. All samples for the iron and zinc analysis were irradiated in the reactor core within site 2A. Within this site, two aluminum canisters may be stacked at a time, each holding 8 sample quartz tubes. Hence, it was important when planning irradiations to ensure that the flux received by the two stacked canisters were equivalent, whereas if they weren't, each can would require different irradiations. For the tissue sample irradiations in this study, the convenient system used to measure the neutron flux received by each can was by pipetting a solution that contained 0.1 μg of cobalt onto filter paper that was thereafter allowed to dry and then wrapped in aluminum foil. This cobalt source was placed vertically in the center, between the two rows in each can before the samples were sent for irradiation.

For the measurement of the thermal flux in the range of interest, that is a neutron flux between 10^{11} and 10^{14} neutrons/cm^2·s, as are seen in the reactor core, a detector material is needed with a simple isotopic composition, with a thermal cross-section of between 1 barn and 100 barns and without large resonances at low energies. The physical and chemical properties that make cobalt a suitable choice are its large thermal neutron cross-section and its long half-life of 5.27 years. For slow neutrons and relatively long irradiations, the ^{59}Co(n, γ) ^{60}Co reaction is superior to all other reactions. With a thermal cross section of 37.13 barns and resonance energy at 1173.24 keV, cobalt fulfills all of these conditions and is the most suitable material for this purpose. By neutron capture, the nucleus ^{60}Co is formed. This nucleus also has an isomeric state at 59 keV with a half-life of 10.5 min. In this study, the short-lived, isomeric state ^{60m}Co, allowed for the quick and efficient determination of whether equivalent amounts of ^{60}Co were pipetted onto each of the filter papers for the flux determination. The weight of cobalt irradiated was a 10 μL droplet of diluted cobalt standard stock solution of 1000 μg/g (Aldrich Materials Science 20, 706-3) that contained 0.1 μg of cobalt.

To ensure that 0.1 μg of cobalt was pipetted onto each filter paper, we irradiated the cobalt filter papers for the short-lived Co-60m isotope. This NAA protocol consisted of a 2 minute irradiation time, followed by a 5 minute delay and a 5 minute counting time. This was to quickly and efficiently verify accurate pipetting of consistent amounts of cobalt from the standard solution. This standardized the aliquots such that the standards with the closest number of counts were then used concurrently when irradiating the tissues samples in the reactor core in order to effectively measure the integrated neutron flux.

After an irradiation of tissue samples, the calculated values of the neutron flux received by the two cans were 1.76×10^{13} and 1.59×10^{13} $\text{neutrons/cm}^2 \cdot \text{s}$. This verified that if at any time, when two canisters were situated in site 2A, the samples in each aluminum can would be exposed to a fairly uniform neutron field and that we could use the same irradiation protocol for both cans.

2.4.3 – Tissue Digestions

During the course of our measurements, we discovered an iron contamination in the quartz tubes we were using. To eliminate the measurement of the quartz iron and zinc content in summation with the samples, the tissue samples after irradiation must be efficiently removed and transferred to inactive sample holders. Hence, prior to measuring the tissue samples, a tissue acid digestion procedure was employed after the iron and zinc sample irradiations in this study.

Using a Piranha etch tissue acid digestion procedure, the active tissue samples were digested and transferred to inactive screw-cap vials. Acidic Piranha Etch is a mixture of two reactive chemicals in volume ratios of 2-4:1 (Clark, 1998). The two components are concentrated sulfuric acid (EMD SX 1244-55, NJ) and 30% hydrogen peroxide (Caledon Laboratory Chemicals 75110, ON). Piranha, in all acidic mixture proportions and types is self-reactive, volatile, corrosive, oxidative and exothermal in nature. It is a very powerful oxidizer and is an excellent solvent for many metals, their salts and an effective glass cleaner for the removal of organic contaminants. In our experiments, the ratio that was found to be most optimal in the tissue digestion yield time was a 4:1 ratio of sulfuric acid to hydrogen peroxide. Furthermore, to increase the yield time of the digestion, the samples were placed in an ultrasonic bath to maintain a slightly elevated temperature after the initial heat of reaction has dissipated (Clark, 1998).

All activated spinal cord tissues for analysis of iron and zinc were digested with the Piranha etch acid solution and transferred from the active quartz using a micropipette, to an inactive screw-cap vial. Once the tissue-acid solution was transferred, an extra wash with additional acid was used to ensure complete removal of any tissue residue remaining in the quartz or pipette.

2.4.4 – Standards and Biological Reference Validation

Standards for the iron and zinc NAA technique were prepared from standard solutions. The standards consisted of 100 μg of iron that was pipetted from a 1000 μg/mL solution (Ultra Scientific Analytical Solutions, K01063, RI) and 100 μg of zinc that was pipetted from a 1000 mg/L standard solution (Fluka Analytical BCBC5944, Switzerland). The iron and zinc standard solutions were combined in a single quartz tube and were irradiated alongside the tissues samples in the reactor core. Two standards were irradiated in each aluminum canister, with a standard in the top and bottom row.

The standards and the spinal cord tissue samples were all freeze dried and thereafter secured by being wrapped in aluminum foil. Once prepared, six spinal cord tissue samples and two standards were packaged into a canister that was then delivered to the reactor core for irradiation. The standards and samples were irradiated in the reactor core for 10 days, with each day having an irradiation time of approximately 14 hours. Following the irradiation period, the samples were removed from the reactor core and were allowed to cool for 10 days prior to handling. Once retrieved from the reactor, the

quartz vials were unpackaged from the aluminum foil, and the tissue acid digestion procedure was carried out on all of the spinal cord tissue samples. After the transfer of the digested tissue samples to inactive screw-cap vials, the samples and standards were measured using an Aptec HPGe spectroscopy system with a counting time of 8 hours (28800 seconds). Two samples were measured in each working day.

The accuracy of this comparative NAA technique for quantification of iron and zinc in spinal cord tissues was validated using the United States' National Institute of Standards and Technology (NIST) certified bovine muscle powder standard reference material (Reference Material 8414). The bovine muscle tissue sample weights were chosen so to simulate the average freeze-dried regional brain region weights to determine whether trace amounts of iron and zinc would be measurable. The certified and experimentally observed concentrations of iron and zinc in the bovine muscle reference material are given below in Table 4, and are in good agreement with one another, though the experimentally determined values were slightly lower than the stated concentrations.

Table 4: Certified and experimental concentrations of Fe and Zn in the NIST bovine muscle powder standard.

Bovine Muscle Tissue Sample	NIST Certified Concentration of Fe [μg/g]	Experimental Concentration of Fe [μg/g]	NIST Certified Concentration of Zn [μg/g]	Experimental Concentration of Zn [μg/g]
Sample #1	71.2 ± 9.2	67.81	142 ± 14	137.11
Sample #2		68.04		132.31
Sample #3		63.15		130.52
Sample #4		60.67		123.86
Sample #5		61.56		125.94
Sample #6		67.14		132.94
	Average	64.73		130.45
	Standard Deviation	3.32		4.85

The validation using the bovine muscle powder reference material in Table 4, illustrates that the experimental NAA values lie well within the certified ranges. A feasible reason for the variations in the measurements is likely the loss of residual tissue during the tissue digestions. The calculated percent difference from the NIST values for iron and zinc are 9.1% and 8.1% respectively. This similarity in percent difference supports the hypothesis of systematic error in the digestion process. Overall, this NAA method was considered accurate for the measurements of iron and zinc in further biological tissue samples. The errors associated with the reported values in Table 4 are as follows – NIST: mean ± uncertainty weight and experimental concentration: mean ± standard deviation (n=6).

Chapter 3 – Animal Methodology

The experiments in this study were carried out with Long Evans (*le*) control and Long Evans shaker (*les*) rats that were bred and raised in the Central Animal Facility at McMaster University by Dr. Jacek Kwiecien. This experiment was approved by the Animal Research Ethics Board at McMaster University. The *les* mutant was first discovered in 1992 at McMaster University, Canada, in a breeding colony of Long Evans (*le*) rats originally derived from a Charles River laboratories breeding stock. These rats are housed under a 12:12-h light:dark cycle and are given rodent chow (Lab Diets, Purina Mills International, St Louis, MO) and tap water ad libitum (Kwiecien, 2010).

For this research, transition metal levels were studied in age groups of 3 and 16 weeks in both the *le* control and mutant *les* strain. However, due to the time restraint and frequency of the reproduction of a sufficient number of control and shaker rats, the experimental analysis in this research was not limited to a certain sex. Furthermore, another difficulty encountered in this study was rearing the *les* rats to 16 weeks. Specifically, dysmyelinated *les* rats are prone to seizures and tonic-clonic convulsions, sometimes resulting in hyperflexion of the spinal column and severe injury to the midthoracic spinal cord. This results in acute hindlimb paralysis requiring immediate euthanasia (Kwiecien, 2010). Therefore, in this study, the animal groups that were investigated were the 3 week *le* and *les* rats with an n=5 for each strain, whereas the study of the 16 week aged rats, consisted of *le* rats with an n=5 while the age matched *les* rats were limited to an n=3.

Once the rats reached the respective ages, the brains were harvested and the distinct regions were dissected. This was important to enable the study of the levels of transition metals regionally, as each brain region has different tissue functions and properties. The regions that were dissected and investigated included the cerebral cortex, cerebellum, corpus callosum, hippocampus, striatum and thalamus, which were most accurately identifiable from the gross anatomy of the rat brain. The spinal cord, blood, and visceral organs were also harvested to further analyze the respective CNS and systemic metal levels. It should be noted that due to the better throughput of the manganese NAA assay, it was possible to measure the manganese concentrations in all of the tissue sample types collected. However, considering the longer throughput for the iron and zinc NAA, due to the longer irradiation and delay time, followed by the tissue digestions and lengthy measurement time, iron and zinc measurements only in the spinal cord tissues to assess the feasibility of those measurements.

Overall, for the experimental methodology in this research, the brain tissue, spinal cord, kidney and liver samples were harvested from the age-matched control and *les* mutant strains at 3 and 16 weeks where they were then prepared for transition metal content measurements. All tissue samples were freeze-dried prior to any analysis. The resulting small samples were then measured for manganese, iron and zinc using neutron activation analysis (NAA).

3.1 – Handling of Rodent Tissue Samples

3.1.1 – Tissue Harvest

At the time of tissue harvest, to avoid altering the metal levels in the samples, there was no tissue fixation utilized (Schrag *et al.,* 2010). During the tissue harvest, each rat was induced and maintained at the surgical anesthetized plane in 100% oxygen and 5% isofluorane. The rat was induced in a chamber and then transferred to a nose cone where deep surgical anesthesia was confirmed via the absence of the paw pinch reflex. A cardiac draw of approximately 0.5 - 1 mL of blood was then obtained, thereby sacrificing the rat. The right kidney and a lobe of the liver was also dissected and stored on ice for the remainder of the procedure. Following the removal of the visceral organs, the rat was decapitated with a surgical scissors and the brain was harvested intact. Immediately after removal, the brain was immersed in isopentane in a liquid nitrogen bath thereby snap freezing it to prevent the diffusion of metal ions across the brain regions. The spinal cord was then carefully separated and removed from the vertebral column. All blood, liver, kidney, whole brain and spinal cord tissue samples were transferred on ice to a freezer where they were stored at -80°C until dissection and sample preparation.

3.1.2 – Brain Dissection

Prior to dissection, the whole brain was partially thawed. Using a surgical scalpel, an initial cut was made at the junction of the cerebellum and the cortex. The cerebral matter was separated and collected for tissue analysis. A bilateral cut was then made at the longitudinal fissure separating the left and right hemispheres. At the posterior end of each hemisphere, the cortex was separated exposing the entire hippocampus, which was removed using a micro spatula. The thalamus was then separated and collected. Next, by separating the cortex at the anterior part of the hemisphere, the entire striatum was exposed for collection. Finally, the frontal cortex was separated from the attached white matter and the region was collected for analysis.

We would like to note that with the *les* brain dissections, it was often difficult to visually distinguish the required brain regions because the brain was missing myelin, which aids in identifying regional borders. However, it was observed, that although the desired regions were not clearly outlined, these brain tissue regions were much easier to separate from the whole brain during the dissections.

3.1.3 –Sample Preparation

For metal analysis brain region tissue samples were transferred to a polyethylene holder for manganese NAA by using a microspatula at the time of dissections. Tissue samples from the harvested spinal cords were also taken for manganese analysis in the

CNS. While for systemic measurements of manganese, portions of tissue from the collected kidneys and livers were collected and put into polyethylene tubes. Similarly, a portion of the spinal cord tissues for the iron and zinc NAA analysis were also collected, but however were placed in the quartz vials. Note that for the spinal cords, the mid-thoracic region was cut for manganese NAA, whereas the lumbar region was isolated for all iron and zinc NAA analysis. Once the wet weight for the NAA samples were recorded, they were kept frozen at -80°C until the freeze-drying procedure.

During irradiation, to prevent water evaporation and pressure build-up in the NAA vials that may cause a rupture and consequent radioactive contamination, all tissue samples must be dehydrated. Therefore, once frozen, all NAA samples were transferred to the freeze-dryer that via reducing the pressure in the chamber, removes the water from the samples through sublimation. Once the freeze-drying was complete, the NAA samples were then sealed in the polyethylene vials for manganese NAA and the quartz tubes with spinal cord samples were wrapped in aluminum foil.

Chapter 4 – Manganese

4.1 – Manganese Measurements Synopsis

In this study we investigated manganese levels systemically and in the central nervous system (CNS) within five 3-week-old *le* control, five 3-week-old *les* mutant, five 16-week-old *le* control and three 16-week-old *les* mutant rats. Manganese measurements were made in the cerebral cortex, cerebellum, thalamus, hippocampus and striatum regions of the brain, as well as in the spinal cord for each of the rats. We also considered manganese levels in kidney and liver tissue samples within each rat to assess possible systemic disruption. Neutron activation analysis was the technique used for the manganese metal measurements.

4.2 – Manganese Statistical Analysis

Statistical analyses were performed using SPSS (IBM SPSS Statistics Version 21.0, IBM Corp.). Data were first assessed for normality using the Shapiro-Wilk test. For normally distributed data, a one-way ANOVA was carried out with age, phenotype, and region as factors. For not normally distributed data, the Kruskal-Wallis test was implemented with the same factors. The Levene Statistic test was used to test for the homogeneity of variances of the metal concentrations across groups. For homogeneous variances, a Tukey HSD post-hoc test was used to test the significant differences in metal concentration between the CNS regions of the 3 week and 16-week-old control and *les* rats. However, when the Levene's test indicated inhomogeneous variances, a Dunnett T3 post-hoc test was applied. This same procedure was also employed to test for significance in the manganese concentrations in the kidney and liver tissues.

In addition, we determined the source of variation in our manganese sample measurements by comparing the sum of variance, calculated using the counting statistic errors, with the sum of squares, calculated from our measured concentration values, in each group. Using the count rate error from sample measurements, and the calculated wet weight concentrations, the sum of variances and the sum of square values were computed for each of the regional groups.

4.3 – Manganese Experimental Results

Consistent with previous studies of *les* rats, it was visually clear that the *les* rats in this research study lacked normal compacted myelin sheaths at 3 weeks and were virtually undetectable in the 16-week-old *les* rats available for analysis. Furthermore, at

the time of sacrifice, it was observed that at 3 weeks, there was no noticeable difference in the control and *les* rat animal weights. However, for the 16-week-old control and age-matched *les* rats, the *les* rats weighed about half as much as the controls of the same sex. Generally, the female *le* and *les* rats had reduced weights compared to the males at both ages.

The spinal cord and regional brain manganese concentrations in the control and *les* rats at the ages of 3 and 16 weeks, as measured with the manganese NAA protocol are given in Figures 4 and 5 respectively. At the age of 3 weeks, it was observed in Figure 4 that the manganese concentrations in the control and *les* rats were overall fairly similar. This is with the exception of the hippocampus where the control rats had a larger mean manganese concentration compared to the *les* rats. However, this was not a statistically significant difference. Overall, there were no statistically significant changes ($p<0.05$) in manganese levels in the control versus the *les* rats.

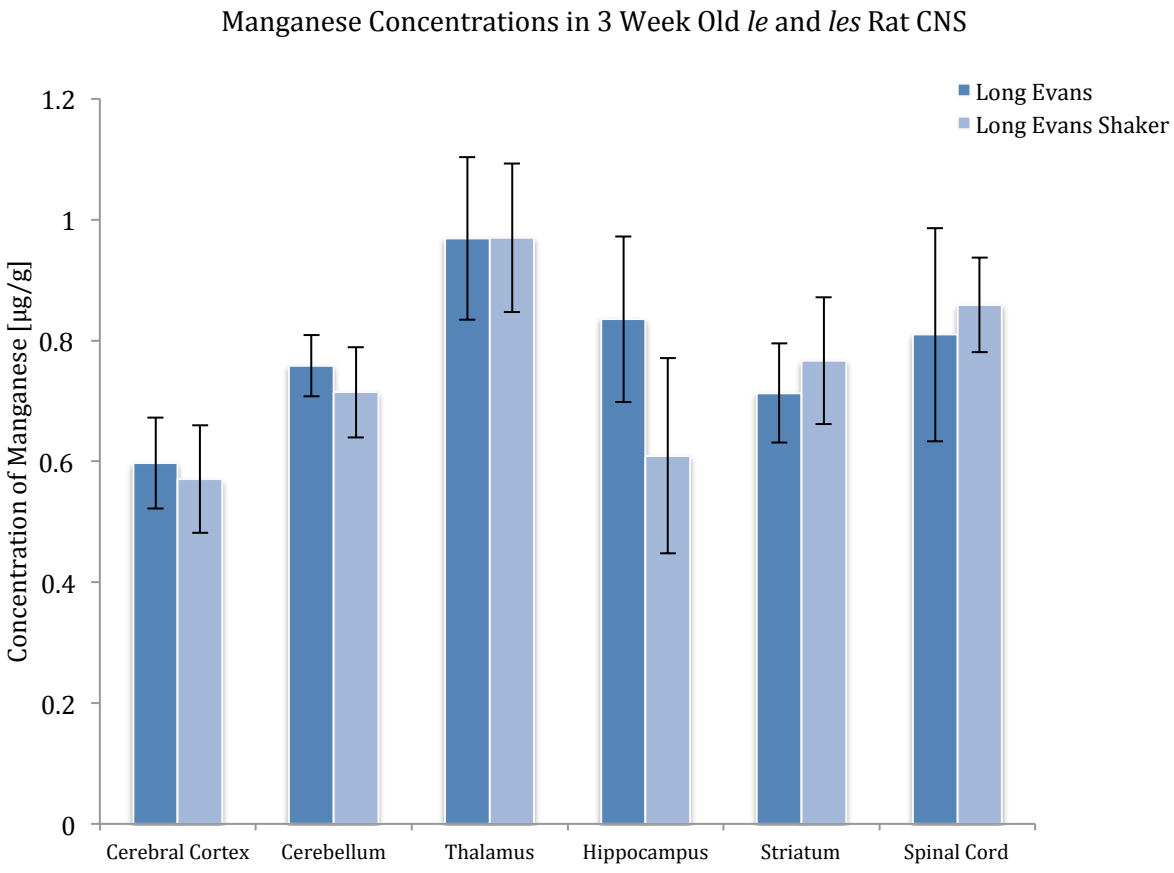

Figure 4: Manganese concentration (mean ± std. dev., n=5 for each group) in the spinal cord and different brain regions of Long Evans control (*le*) and Long Evans Shaker (*les*) rats at 3 weeks of age. Mn concentration was determined using comparative NAA.

In the 16-week-old control and *les* rats, there was a higher trend in manganese concentrations in the cerebellum, thalamus and spinal cord tissue samples as shown in Figure 5. The manganese concentration was significantly higher in the *les* rat cerebellum than in the age-matched control cerebellum. However, the large concentration in the 16 week old control striatum shown in Figure 5 below, although may appear of significance, is not, due to a significantly large sample outlier within the group. This also explains the large standard deviation illustrated. Although not as intense of a difference, due to an outlier measurement, this is the similar case that is observed within the 16-week-old *les* spinal cord.

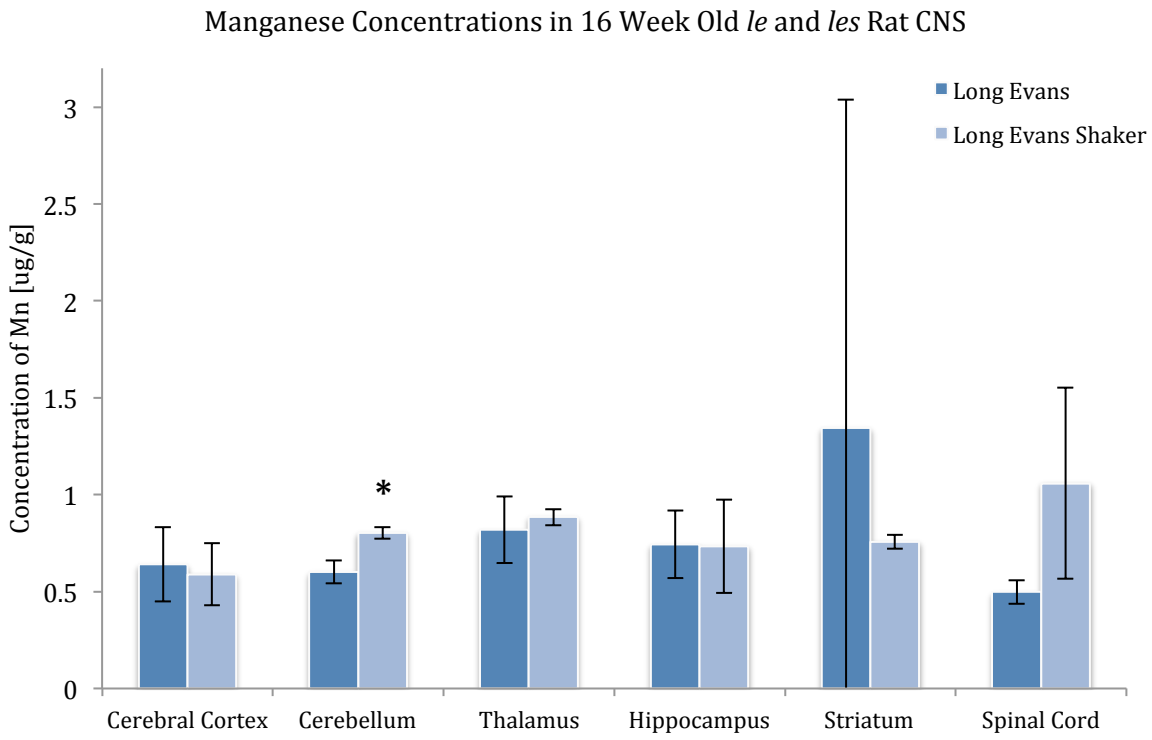

Figure 5: Manganese concentration (mean ± std. dev., n=5 for the Long Evans control group, and n=3 for the Long Evans Shaker group) in the spinal cord and different brain regions of Long Evans control (*le*) and Long Evans Shaker (*les*) rats at 16 weeks of age. Mn concentration was determined using comparative NAA. Statistical significance between the control and *les* regions at $p<0.05$ is denoted by the * symbol.

To assess the systemic manganese levels in the control and *les* rats, manganese was also measured in the visceral organs as shown in Figures 6 and 7. In the kidney and liver, at ages 3 and 16 weeks, the manganese concentrations remained the same and were not significantly different ($p<0.05$) between the control and *les* rats.

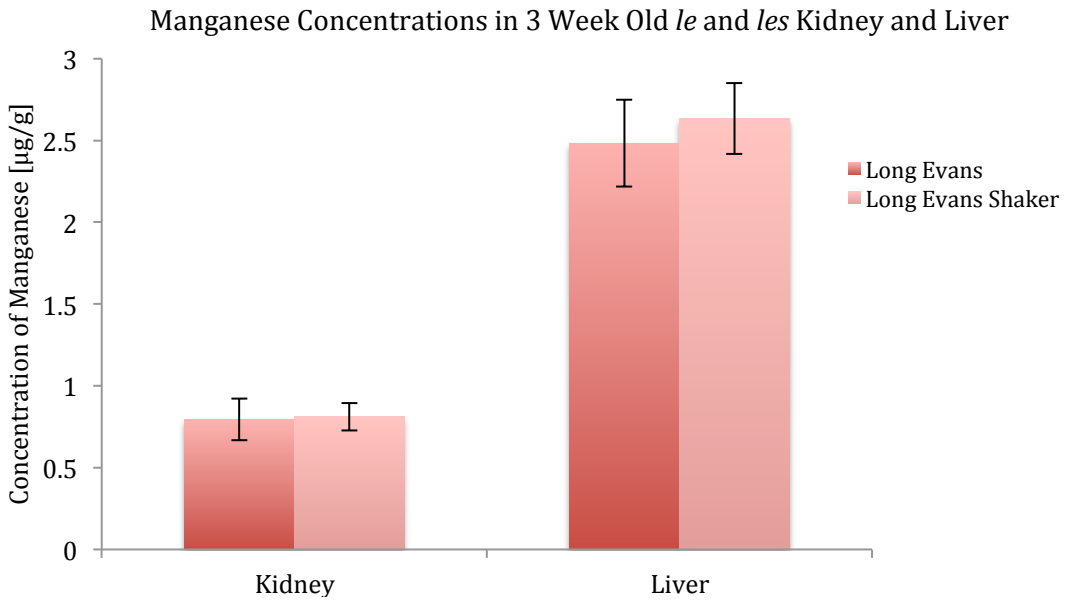

Figure 6: Manganese concentrations (mean ± std. dev., n=5 for each group) in the visceral organs of the *le* control and *les* rats at 3 weeks of age. Manganese concentrations were determined using comparative NAA. There was no statistical significance ($p>0.05$) between control and *les* rats.

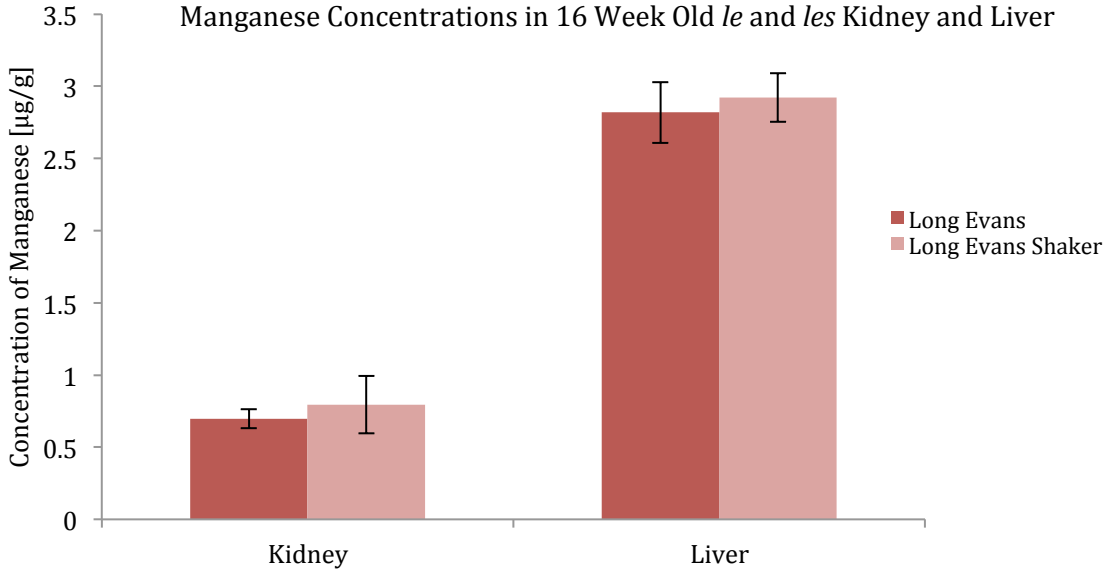

Figure 7: Manganese concentrations (mean ± std. dev., n=5 for the Long Evans control group, and n=3 for the Long Evans Shaker group) in the visceral organs of the *le* control and *les* rats at 16 weeks of age. Manganese concentrations were determined using comparative NAA. There was no statistical significance ($p>0.05$) between control and *les* rats.

Overall, since we only obtained three 16-week-old *les* rats, rather than five, it was important to ensure that efficient measurements were made and that any variations stemming from possible counting statistic errors were reduced. In this study, to determine the sources of variability within the various tissue regions, especially in groups where there were noticeable outlier measurements present, the sum of variance and the sum of square values were computed. This was to determine the proportion of variation associated with the counting method versus actual fluctuations in metal concentrations across matched tissue samples. For the manganese measurements made across all the tissue regions in the 3 and 16-week-old control and *les* rats, the sum of variances/sum of squares ratio ranged from 0.03/11.5 to 0.02/0.002. Although the highest end of the ratio comparison demonstrates variability from the counting statistics, analysis across all of the samples groups suggests that the major source of variation in our measured values is coming from actual variation in tissue concentration within each group. This is likely arising from biological variability and errors in dissections and tissue sample weight measurements.

4.4 – Manganese Discussion

The myelin sheath is essential for the rapid conduction velocity of the nerve fiber via saltatory conduction and can aid in maintaining axonal integrity. Animal models with mutations in myelin genes have been essential for elucidating the role of several proteins that are critical for myelin development and maintenance. The Long-Evans shaker (*les*) rat is one such mutant that has an abnormal insertion in the gene that encodes myelin basic protein (*mbp*). This mutation disrupts the translation of functional *mbp* that results in myelin sheaths that are loosely wound and poorly compacted. Myelin basic protein is an important structural component of the myelin sheath and has also been shown to play a role in the transport and assembly of myelin sheath lipids and proteins. At peak myelin development (2 weeks), *les* mutants develop thin, uncompacted myelin sheaths. Most of this myelin is lost by 4 weeks, and by 8 weeks scarce myelin is present within the CNS of *les* rats (Smith, Mayer & Duncan, 2013).

Studies have illustrated that the *les* rats have numerous microglial cells that are activated as an immune response and hypertrophic astrocytes rich in glial filaments that appear in clusters adjacent to degenerating olgiodendrocytes (OL) (Delaney *et al.,* 1995). However, because the hypomyelination precedes the astrocytic proliferation, it is not believed that these astrocytic processes separated the OLs from the axons they are to myelinate. Therefore, along with abnormal, vacuolated microglial cells and the axonal swellings and spheroids seen by microscopy, the astrocytic changes are considered to be secondary to dysmyelination (Delaney *et al.,* 1995; Dentinger, Barron & Csiza, 1982). In addition, in the *les* rat, astrocyte processes are abundant in all CNS tissues, with an obvious increase in glial filaments. Specifically, studies have found intense gliosis marked by the proliferation and hypertrophy of glial cells including astrocytes, microglia and oligodendrocytes, in the brain and spinal cord of the *les* rat (Kwiecien *et al.,* 1998).

Immunolabelling of microglia was highest in intensity in white and gray matter in *les* spinal cord (Schulz *et al.,* 2011). In addition, in the *les* rats, axons grow in diameter similar to controls between 2 and 16 weeks and appear normal ultrastructurally, with only occasional scattered, degenerating axons being seen (Kwiecien *et al.,* 1998).

Therefore, the distinct lack of myelin in the CNS coincides with astrogliosis, resulting in the enveloping of small bundles of naked axons by hypertrophied astrocyte processes that separate the axonal bundles from each other in *les* rats. Although the precise mechanisms of astrogliosis in which hypertrophied astrocyte processes separate bundles of naked axons are unknown, this reaction can be considered compensatory for lack of myelin and an attempt to isolate naked axons (Kwiecien, 2010). Proliferation of glial cells with increased mitotic activity is another important cellular compensatory mechanism in the CNS. In adult *les* rats mitotic activity increases at 12 weeks and peaks at 16 to 20 weeks of age (Kwiecien, 2010). Studies in the optic nerve of control rats have found that the total number of glial cells reached approximately 300 cells at 8 weeks of age and then gradually decreased to approximately 240 cells by the age of 40 weeks. In contrast, the numbers of glial cells in the optic nerve of the *les* strain increased at a greater rate and for a prolonged period of time, reaching approximately 700 cells at 16 weeks of age and then remaining fairly constant (Kwiecien, 2010).

Evidence shows a strong relationship between manganese and astroglia, as around 80% of manganese in the brain is associated with the neurotransmitter regulator glutamine synthetase (Wedler & Denman, 1984), which is located primarily in astroglia *in vivo* (Carl *et al.,* 1993; Kawai *et al.,* 2010). Glutamine synthetase (GS) is an astrocytic-specific enzyme that metabolizes the neurotransmitter glutamate to glutamine. GS contains eight manganese ions per octamer, thus accounting for the majority of total brain manganese (Aschner, Gannon & Kimelberg 1992; Erikson *et al.,* 2004). The results in this work support the correlation between increased astrocytic activity and manganese metal levels. Brain manganese is preferentially deposited in astrocytes given the presence of high-capacity transporters within these cells. The concentration of manganese in astrocytes is 50-60 times higher than in neurons (Aschner, Gannon & Kimelberg 1992; Sidoryk-Wegrzynowicz & Aschner, 2013b). This hypothesis explains the overall elevated trend in manganese concentrations in this study in the *les* CNS compared to the 16-week-old age-matched controls. Therefore, increases in manganese levels may represent an important pathological event associated with astrogliosis in the pathogenesis of neurological disorders.

Furthermore, a study with immunostaining of *les* sagittal brain and transverse spinal cord sections has indicated that reactive microglia and astrocytes are located in white matter areas such as the olfactory tract, corpus callosum, cerebellum, brain stem and spinal cord (Zhang *et al.,* 2001). This supports our research finding, where there was a significant ($p<0.05$) increase in manganese levels in the 16-week-old *les* rat cerebellum in comparison to the age-matched control cerebellum. In addition, although not statistically significant, a greater increase in the manganese concentration in the 16-week-old *les* rat spinal cords compared to the control spinal cords was also observed. Research has also shown that in the control rat CNS, reactive microglia are displayed in both gray

and white matter from 2 weeks of age. In normal cerebellum, the microglial cell density in the white matter is eight times as high as in gray matter at 1 week of age. This ratio decreases progressively to 2:1 at the end of 4 weeks of life, and is then maintained through 16 weeks. However, in the *les* cerebellum, the morphology and density of microglia in both white and gray matter are similar to findings in normal rats in the first week (Zhang *et al.,* 2001). In areas with intermixed gray and white matter, such as the striatum, research shows reactive microglia and astrocytes have been found to appear only along the axonal tracts that are normally myelinated (Zhang *et al.,* 2001). This is consistent with the findings in this thesis which shows either lower or corresponding manganese levels in the control and *les* rat intermixed gray and white matter regions such as in the cerebral cortex, hippocampus and striatum.

It has been shown that the processes mediating the brain influx of physiological manganese concentrations are primarily through the BBB and are non-saturable. For instance, manganese uptake into the choroid plexus (CP) ventricles of the brain where cerebrospinal fluid is produced is greater than into various brain regions. However, uptake into the cerebrospinal fluid (CSF) is lower than into the brain, illustrating that manganese enters the brain primarily through the BBB. Overall, there appears to be multiple mechanisms mediating manganese brain uptake across the BBB, including uptake of the manganese transferrin complex presumably by transferrin receptor-mediated endocytosis (TfR-ME), as well as more than one process to take up manganese that is not associated with transferrin. Whereas results from studies suggest that diffusion mediates brain manganese efflux (Yokel, 2006). Such findings as these suggest that it is more probable to associate the elevated manganese levels in neurodegenerative diseases due to an increase in astrocytic activity.

Therefore, from numerous studies, manganese has been associated with over-activation of glial cells, namely astrocytes and microglia (Liu *et al.,* 2009; Spranger *et al.,* 1998). Microglia and astrocytes normally have diverse beneficial functions essential for neuronal survival and importantly astrocytes have the ability to influence myelination by oligodendrocytes (Ishibashi *et al.,* 2006); but over-activation of these cells is highly detrimental and neurotoxic (Zhao *et al.,* 2009). Specifically, manganese activated astrocytes and microglia release various non-neuronal reactive oxygen species and numerous inflammatory mediators that contribute to degeneration of brain cells via oxidative stress (Aschner *et al.,* 2009; Filipov & Dodd, 2012). In addition, manganese is highly toxic to astrocytes themselves because the metal accumulates in astrocytes in amounts 50 times greater than in neurons and severely disrupts astrocytic energy metabolism (Aschner, Gannon & Kimelberg, 1992). In demyelinating diseases, the dysfunctional astrocytes may contribute to axonal loss and demyelination through oligodendrocyte damage leading to impaired myelination (Cambron *et al.,* 2012).

Overall, in this research, the results from the manganese metal measurements in the central nervous system and visceral organs of *le* and *les* rats at 3 and 16 weeks of age verified that the *les* rat mutation is strictly an autoimmune CNS disease. In particular, the consistent levels of manganese concentrations within the kidney and liver seen in this work illustrated that the dyshomeostasis in manganese levels in especially the older *les*

rats is confined to the CNS. These results supported the studies that have shown an increased proliferation of astrocytes in the *les* rat CNS, leading to astrogliosis, which is associated with manganese uptake and accumulation. Therefore, in responding to the severe dysmyelination and oligodendroglial pathology in the *les* rats, microglia proliferate and morphologically transform, such that the lack of myelin in the CNS coincides with astrogliosis. This results in the enveloping of small bundles of naked axons by hypertrophied astrocyte processes, which effectively separate the axonal bundles from each other in *les* rats (Tarohda, Yamamoto & Amamo 2004; Zhang *et al.,* 2001). This therefore concurrently results in an increase in manganese metal concentrations in white matter regions as was marginally demonstrated in this thesis. From the preliminary results in the 3 *les* rats at 16 weeks of age that were measured, it can be safely assumed that a stronger observation of increased manganese levels in the CNS regions would be illustrated.

Chapter 5 – Iron and Zinc

5.1 – Iron and Zinc in Measurements Synopsis

For this experiment, we investigated iron and zinc levels in the spinal cords of five 3-week-old *le* control, five 3-week-old *les* mutant, five 16-week-old *le* control and three 16-week-old *les* mutant rats. In particular, iron and zinc measurements were made in the spinal cord for each of the rats. Neutron activation analysis was the technique used for these metal measurements.

5.2 – Iron and Zinc Statistical Analysis

Statistical analyses were performed using the SPSS (IBM SPSS Statistics Version 21.0, IBM Corp.). Data were first assessed for normality using the Shapiro-Wilk test. For normally distributed data, a one-way ANOVA for each metal measurement was carried out with age and phenotype as factors. For not normally distributed data, the Kruskal-Wallis test was implemented with the same factors. The Levene Statistic test was used to test for the homogeneity of variances of the metal concentrations across groups. For homogeneous variances, a Tukey HSD post-hoc test was used to test the significant differences in iron and zinc metal concentrations between the spinal cord regions of the 3 week and 16-week-old control and *les* rats. However, when the Levene's test indicated inhomogeneous variances, a Dunnett T3 post-hoc test was applied.

In addition, we determined the source of variation in our iron and zinc sample measurements by comparing the sum of variance, calculated using the counting statistic errors, with the sum of squares, calculated from our measured concentration values, in each group. Using the count rate error from sample measurements, and the calculated wet weight concentrations, the sum of variances and the sum of squares values were computed for each of the spinal cord groups.

5.3 – Iron and Zinc Experimental Results

The iron and zinc concentrations within the spinal cord in the control and *les* rats at the ages of 3 and 16 weeks, as measured with the iron and zinc NAA assay are given in Figures 8 and 9 respectively. At the ages of 3 and 16 weeks, it was observed in Figure 8 that the iron concentrations in the *les* rats had an overall higher concentration, with a slightly more noticeable difference in the 16-week-old *les* rats. However there was no statistical significance ($p<0.05$) found between the groups.

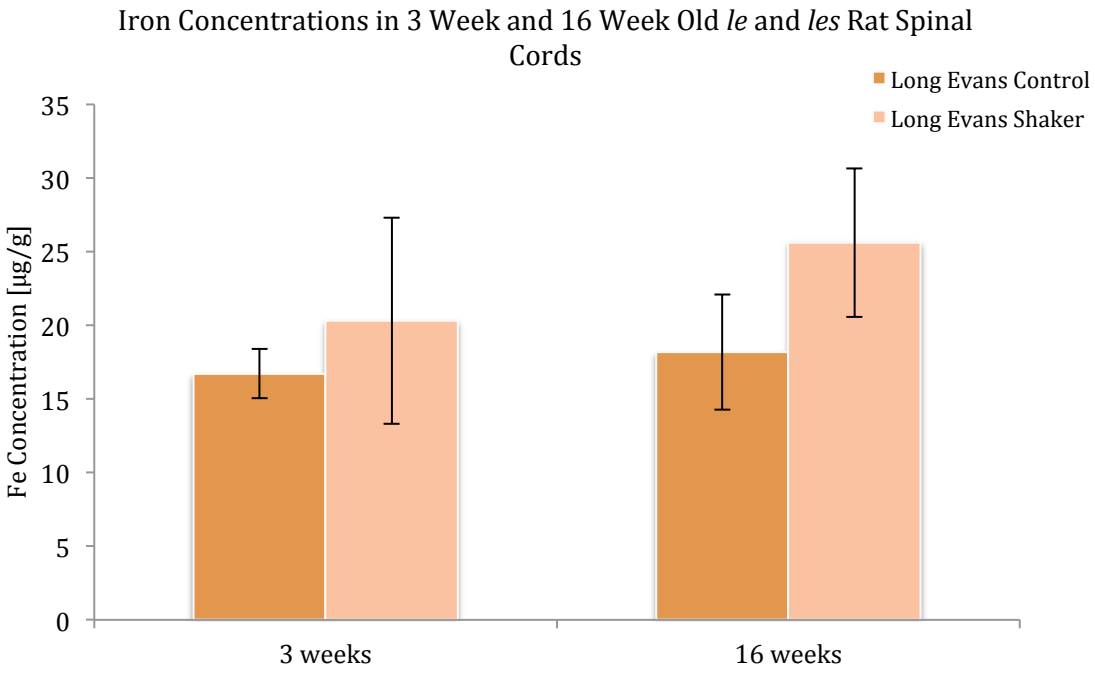

Figure 8: Iron concentration (mean ± std. dev., n=5 for the Long Evans control group, and n=3 for the Long Evans Shaker group) in the spinal cord of Long Evans control (*le*) and Long Evans Shaker (*les*) rats at 3 and 16 weeks of age. Fe concentration was determined using comparative NAA.

Figure 9 illustrates the zinc concentration levels within the spinal cord of the control and *les* rats at 3 and 16 weeks. The zinc measurements demonstrate a slightly elevated level in the 3 week old *les* rats, with however a significant increase ($p<0.05$) in concentration within the 16-week-old *les* rat spinal cords in comparison to the age-matched controls.

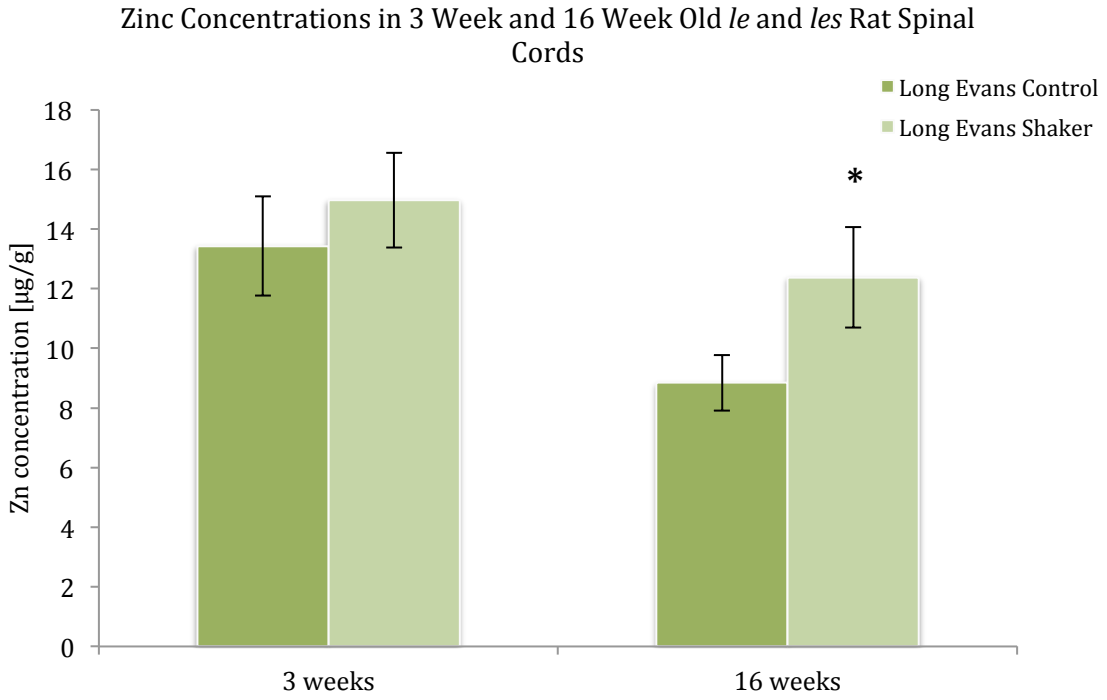

Figure 9: Zinc concentration (mean ± std. dev., n=5 for the Long Evans control group, and n=3 for the Long Evans Shaker group) in the spinal cord of Long Evans control (*le*) and Long Evans Shaker (*les*) rats at 3 and 16 weeks of age. Zn concentration was determined using comparative NAA. Statistical significance between the control and *les* spinal cord tissues at $p<0.05$ is denoted by the * symbol.

Overall, since we only obtained three 16-week-old *les* rats, rather than five, it was important to ensure that efficient measurements were made and that any variations stemming from possible counting statistic errors were reduced. In this study, to determine the sources of variability within the spinal cord tissues, especially in groups where there were noticeable outlier measurements present, the sum of variance and the sum of square values were computed. This was to determine the proportion of variation associated with the counting method versus actual fluctuations in metal concentrations across matched tissue samples. For the iron measurements made in the spinal cord tissues in the 3 and 16-week-old control and *les* rats, the sum of variances/sum of squares ratio ranged from 2.85/195.77 to 2.88/11.07. Whereas for the zinc levels measured in the spinal cord tissues, the sum of variances/sum of squares ratio ranged from 0.03/11.06 to 0.02/3.45. These calculations suggest that the major source of variation in our measured values is coming from actual variation in tissue concentration within each group. This is likely arising from biological variability and errors in dissections and tissue sample weight measurements.

5.4 – Iron and Zinc Discussion

Chronic demyelination of the central nervous system (CNS) results in axonal degeneration and permanent loss of function. Demyelination in the CNS is associated with a wide variety of disorders that either directly or indirectly induce oligodendrocyte (OL) injury or loss. Oligodendrocytes are cells that produce myelin and construct myelin sheaths around the axons in the CNS. They actively maintain myelin throughout life and function as an insulator to assist axons in the rapid conduction of axonal action potentials. Myelin is a composite of proteins, cholesterol, glycolipids, phosphoglycerides, and sphingomyelins (Zhang *et al.,* 2001).

It is known that iron is required for myelination processes since a decreased availability of iron in the diet is associated with hypomyelination (Lozoff & Georgieff 2006). Iron is abundant in various types of cells in the CNS, with the highest concentrations found in the astrocyte and oligodendrocyte glial cells (Rouault & Cooperman, 2006). Astrocytes are thought to function in iron storage and regulation in the CNS, whereas oligodendrocytes synthesize high levels of ferritin and therefore not only have the highest iron content of all CNS cell types, but also possess a high buffering capacity for iron (Rouault & Cooperman, 2006). As myelination continues during adulthood, iron is continually required for myelin production and maintenance. Hence, accumulations of ferritin in oligodendrocytes could correspond to the general task of ferritin to store iron in a non-toxic form (Quintana & Gutierrez, 2010).

In *les* rats, numerous studies illustrate that actively myelinating oligodendrocytes show remarkable degenerative changes. The structural changes in the *les* rat OLs indicate an abnormal accumulation of a metabolite feasibly involved in the formation of myelin. In particular, the loss-of-function mutation in the myelin basic protein gene of *les* rats correlated with metabolically active oligodendrocytes. Unsuccessful attempts at myelination coincide with ultrastructural pathology characterized by progressive accumulation of membranous material in the perikaryon, which is the bulbous end of the neuron containing the cell nucleus. The progression in the pathology of *les* oligodendrocytes suggests that abundant metabolic activity designed to rapidly form vast quantities of myelin is not shut down at the end of the neonatal stage, as in normally myelinating rats, but remains vigorous in *les* rats. The progressive accumulation of membranous material in the form of vesicles contributes to the abnormal enlargement of the perikaryon (Kwiecien, 2010). It has been hypothesized that the inability of OL to establish receptor-mediated functional contact with the axons may result in the lack of formation or significantly impaired formation of myelin sheaths. Yet, precursor components of myelin may be produced continuously, resulting in their accumulation in organelles and overall swelling of the OL (Delaney *et al.,* 1995). Although failure of production of compact myelin may lead to the accumulation of transport vesicles within the cytoplasm, they do not appear to lead to oligodendrocyte or abnormal cell death in *les*. Rather there appears to be an increase in mature oligodendrocytes in older animals (Kwiecien *et al.,* 1998).

Generally, oligodendrocytes increase in number in the normal CNS during myelination and many undergo apoptosis shortly after myelination is complete (Badaracco, Siri & Pasquini, 2010). In *les*, however, where the myelin sheaths are loosely wound and poorly compacted, more oligodendrocytes survive after myelination ceases (Kwiecien *et al.,* 1998). As aforementioned, most of these oligodendrocytes contain abnormal inclusions. Alternatively, this oligodendroglial pathology may lead to the breakdown of abnormal myelin sheaths due to the result of the elevated microglial reaction. Specifically, in *les* rats, as a sensor of CNS homeostasis, microglia increase in number accordingly during the first month of age. However, reactive microglia are not expressed until the stage when the mutant oligodendrocytes accumulate vesicles in their cytoplasm resulting in cell dysfunction. Studies suggest that this progressive oligodendroglial pathology is likely the trigger for further microglial activation (Kwiecien *et al.,* 1998). The microglial activation may lead to the astrocytic reaction through paracrine interactions as seen in the *les* white matter (Kwiecien *et al.,* 1998; Zhang *et al.,* 2001). In addition, research also shows that traumatic contusive injury to the blood-spinal cord barrier results in an initial acute presence of iron at the lesion epicenter (Quintana & Gutierrez 2010).

This study investigated the iron and zinc levels in *le* and *les* rat spinal cords at the ages of 3 and 16 weeks. In the *les* spinal cord, scattered, thinly myelinated fibers are present at 3 weeks of age. However, at 16 weeks of age, no myelin sheaths are observed in the spinal cord, indicating a loss of myelin overtime. Studies of ultrastructural examination of thin sections from the ventral column of the spinal cord confirm the scarcity and then loss of myelin with time where many scattered axons in the spinal cord were noted to be ensheathed by non-compacted lamellae in the *les* rat at 2-4 weeks of age. Yet, most importantly, the myelin that is present at all ages examined is abnormally compacted and lack a major dense line, in contrast to control CNS myelin (Kwiecien *et al.,* 1998). The results from this research show that although not statistically significant, there was a noticeable trend of increased iron concentrations in the 3-week and 16-week-old *les* rats while there was a significant ($p<0.05$) increase in zinc concentration in the 16-week-old *les* rats. Once again, it should be noted that the metal measurements in this study were limited (n=3) due to the rearing difficulty of *les* rats to 16 weeks of age.

The generation and function of oligodendrocytes are known to be dependent on iron availability. Specifically, studies have found that oligodendrocyte precursor cells (OPCs) have a greater need to acquire and retain iron for their proliferation and differentiation into oligodendrocytes as well as for myelination. The time point at which the maximum amount of myelin is being produced coincides with a peak period of iron influx into the brain and cerebrospinal fluid. It has been suggested that this increase in iron uptake is a necessary step to proceed through gliogenesis and is tightly linked with the normal production of myelin in the brain (Morath & Mayer-Proschel, 2001). After the completion of myelination, oligodendrocytes likely require less iron and maintain stable iron levels through iron efflux (Magaki *et al.,* 2007). In addition, it has been revealed that OPC cells exposed to high iron, drop out of division without a corresponding initiation of differentiation. This suggests that increased iron levels, such as might be found during the peak in iron uptake, may be a way of limiting the number of cells capable of generating

an oligodendrocyte in preparation for differentiation without promoting the actual transition (Morath & Mayer-Proschel, 2001).

It is hypothesized that the presence of ferrous iron in ferritin cores from oligodendrocytes are a source of oxidative stress that may lead to myelin damage and has been reported in elderly people and especially in AD patients. Furthermore, it has also been observed that patients suffering from neurological diseases accumulate iron in the brain regions affected by the disease. Specifically, studies have shown an increased activity of antioxidant proteins in the brains of AD patients, especially in the hippocampus where iron is accumulated (Quintana & Gutierrez, 2010). Despite stringent regulation of iron within the CNS, iron accumulation occurs gradually over time with concurrent increases in ferritin. CNS iron accumulation may induce neuronal damage even after it has become bound to ferritin because iron can also be released in its ferrous form under the acidic conditions present in extracellular fluid (Gaasch *et al.,* 2007).

Similar to iron, zinc is also a divalent cation that has long been implicated in a myriad of cellular processes. For zinc, these processes range from interactions with zinc-finger proteins and protein kinases to modulation of ion channels. In the CNS, zinc localizes to numerous pathways. Most notably, zinc has been shown to localize within the axon terminals of dentate granule cells located in the hippocampus (Cole *et al.,* 1999). Furthermore, given that zinc is co-released with the glutamate neurotransmitter, on high-frequency stimulation of axon terminals, this heavy metal's presence in these excitatory synapses is of great physiological importance in the modulation of function at synapses. Studies have shown that, rather than inhibiting, zinc enhances neuronal excitability and strongly potentiates excitotoxicity (Lin, Cohen & Coulter, 2001). In addition to possessing a potential neuromodulator role, excessive Zn^{2+} release occurring during acute CNS injury is also reported to play an important role in inducing neuronal cell death (Law *et al.,* 2003).

While it is clear that zinc can have powerful effects on neuronal metabolism, it is evident that zinc may also have important effects on astrocytic ATP production. Specifically, studies on brain ischemic episodes, characterized by the reduced blood flow to brain tissues, show that ATP reductions caused by intracellular zinc accumulation in turn lead to impaired astrocytic glutamate uptake. This is an effect that could significantly increase excitotoxic components (Dietz, Weiss & Shuttleworth, 2008). Zinc also plays a part in the activation of the microglial resident immune cells of the CNS, contributing to late stages of injury after an ischemic episode (Shuttleworth & Weiss, 2011). With waves of synaptic Zn^{2+} release accompanying spreading depolarizations in a brain-slice model of ischemia, such events may release substantial amounts of Zn^{2+} into the injured brain (Shuttleworth & Weiss, 2011). While experiments have shown that the rat blood-brain barrier to zinc is low, studies of zinc distributions in the brain *in vivo* show a regional distribution with low levels in white matter and relatively high levels in choroid plexuses, cerebral cortex and particularly the dentate gyrus within the hippocampus where zinc is thought to act as neuromodulator agent (Corniola *et al.,* 2008; Franklin, Pullen & Hall, 1992; Law *et al.,* 2003; Yanik *et al.,* 2004).

The significant ($p<0.05$) increase in zinc levels in the available *les* rat spinal cord samples at 16 weeks of age was not unexpected since *les* rats frequently experience tremors and seizures. More specifically, in the CNS, zinc occurs in two forms: the first being tightly bound to proteins and, secondly, the free, cytoplasmic, or extracellular form found in presynaptic vesicles (Szewczyk, 2013). For instance, under clinical conditions such as traumatic brain injury, stroke or epilepsy, the excess influx of zinc into neurons has been found to result in neurotoxicity and damage to postsynaptic neurons (Szewczyk, 2013). However, there have been limited studies with conflicting results that measured zinc levels in different strains of rats/mice and following varying treatment regimes. For instance, there is evidence suggesting that a deficiency, rather than an excess of zinc leads to an increased risk for the development of neurological disorders. Zinc deficiency has been shown to affect neurogenesis and increase neuronal apoptosis, which can lead to learning and memory deficits (Szewczyk, 2013). However, in the *les* rats, research has found that axons appear normal ultrastructurally, with only occasional scattered, degenerating axons being seen (Kwiecien *et al.,* 1998). This research study therefore further supports that the observed increase in zinc concentration in the *les* rat spinal cord tissues at 16 weeks of age may be due to extracellular accumulations in the presynaptic vesicles.

In addition, zinc has been suggested as a positive factor in healthy ageing through the reduction of inflammation (Kahmann *et al.,* 2008). In particular, zinc has been found to have anti-inflammatory properties, such that intracellular zinc has been found to play a key role in signaling immune cells, whereas a low zinc status is associated with increased susceptibility to infection (Haase and Rink 2009; Hasan, Rink & Haase, 2013; Szewczyk, 2013). It is proposed that synaptic zinc release is a key factor in stimulating neurogenesis (Morris & Levenson, 2012). In this study, this suggests that the elevated zinc levels observed in the *les* spinal cord tissues at 16 weeks of age may also be a result of the autoimmune response resulting in the glial activation and inflammation of the microglial, astrocyte and oligodendrocyte cells in an attempt to reduce the inflammatory response. Furthermore, *in vitro* studies have shown that zinc increases the overall accumulation of manganese (Garcia *et al.,* 2006). Therefore it is also not surprising that manganese and zinc are increased in the CNS of the *les* rats observed in this study.

Overall, the mechanism of neurotoxicity in the CNS autoimmune disease in the Long Evans Shaker (*les*) rat is quite complex. The results from the analysis of iron and zinc metal levels in the spinal cord tissue samples from the control and age-matched *les* rats illustrated that there was a higher trend in iron concentration at 16 weeks of age which may correspond to the increased proliferation of iron-dependent oligodendroglial cells. In addition, there was a significant ($p<0.05$) increase in zinc concentration in the 16 week old *les* spinal cords that possibly correlates with excess zinc release in the presynaptic vesicles as is observed in numerous seizure-prone neurodegenerative disorders. Yet, this increase in zinc may also be a result of the neuro-inflammation in the *les* CNS. Zinc is an essential trace element, whose importance to the function of the CNS is increasingly being appreciated. Alterations in zinc dyshomeostasis has been suggested as a key factor in the development of several neuropsychiatric disorders. Therefore, the biological significance of being able to detect and monitor iron and zinc content, in

particular the abnormal accumulation in reactive glial cells, was further highlighted in a study in which this pathological feature was indeed linked to oxidative stress (Quintana & Gutierrez, 2010). However, further studies are required to follow-up on the nature of zinc in biological tissues and its role in neurodegenerative diseases.

Chapter 6 – Future Works and Conclusions

6.1 – Future Works

This study investigated the loss of manganese, iron and zinc transition metal homeostasis in the dysmyelinated Long Evans Shaker (*les*) rat model. Manganese was investigated in the CNS as well as systemically, while iron and zinc concentrations were analyzed in the spinal cord tissue samples. Overall, there was an increased trend in manganese, iron and zinc concentrations most observable in the 16-week-old *les* rats. Of most importance is the result that in these rats we found significant increased levels of manganese in the cerebellum as well as increased zinc concentrations in the spinal cord – both regions with high myelin contents in normal rats. However, due to breeding limitations, raising the *les* rats to 16 weeks of age and the time constraint, this study was limited to an n=3 for the 16-week-old *les* rats. This restricted efficient analysis of transition metal concentrations in most of the tissue regions and limited detections of statistical significance where there were outliers that often resulted in large standard deviations. Therefore, to verify the observations in this study, the next step would be not only obtaining two more 16-week-old *les* rats, but to also increase the overall number of rodent subjects throughout all the groups. From the work in this thesis, we are convinced that this would further validate the observed trend in increased transition metal levels within the CNS of the *les* dysmyelinated rodent model.

Moreover, to further develop the analysis of transition metals in this study, improvement of the throughput of the NAA assay that was used to measure manganese, and especially iron and zinc should be considered. In particular, to enhance the manganese measurements, a longer period of counting would be optimal to reduce errors in counting. Whereas for improving the iron and zinc metal analyses, this would require obtaining quartz tubes with no trace amounts of iron or zinc present. This would eliminate the tissue acid digestion procedure. Furthermore, this would also eliminate the loss of any tissue as may be encountered during the transfer of the digested tissue samples. In addition, the throughput time could also be decreased with additional HPGe detectors. This would provide the ability to measure more than one sample simultaneously and would therefore also decrease the length of time required to obtain all the sample measurements. With an improved NAA assay to measure iron and zinc, this would permit the measurements of these transition metals in the kidney, liver and brain tissue regions. Overall, these suggested improvements in the methods of analysis would greatly advance the ability to elucidate changes in manganese, iron and zinc metal concentrations in the *les* rodents that exhibit progressive dysmyelination, and it will also allow for efficient transition metal analyses of neurodegenerative diseases in human CNS tissue samples.

Alternatively, the measurements of iron and zinc could also be measured using X-ray fluorescence. X-ray fluorescence is another non-destructive technique that enables

simultaneous multi-elemental analysis. This technique is based on the principle that individual atoms, when excited by an external energy source, emit X-ray photons of a characteristic energy or wavelength. By counting the number of photons of each energy emitted from a sample, the elements present may be identified and quantified (University of Missouri, 1996).

6.2 – Overall Conclusion

This thesis demonstrated the measurement of manganese, iron and zinc transition metal levels in the dysmyelinated Long Evans Shaker (*les*) rat and its control counterpart. These measurements were made in an effort to further advance the understanding of the role of transition metal levels in related demyelinating neurological disorders. NAA techniques were successfully applied to measure the metal levels in the rodent tissue samples. The results from the manganese measurements demonstrated an overall regional increased pattern that confirms previous work (Zhang *et al.,* 2001), with however only a significant increase noted in the cerebellum of the 16 week old *les* rats. This verified that increased manganese levels are associated with astrogliosis, which is located to white matter areas in this rodent model of dysmyelination (Zhang *et al.,* 2001). Whereas for iron and zinc that were measured in the spinal cord tissues, there were also overall increased levels of these metals in the *les* mutant strain when compared to the controls, although only significant increases in zinc concentration within the 16 week old *les* spinal cords. The overall trend in increased iron in the *les* rats may suggest the oligodendrocyte cells attempt myelination, since it has been shown that iron increases during myelin formation (Morath & Mayer-Proschel, 2001). While the significant increase in zinc that was observed may correlate with the extracellular accumulations in the presynaptic vesicles due to the tremors and seizure episodes often experienced by the *les* rodents. Yet, the increase in zinc may also result from efforts to reduce neuro-inflammation within the *les* rat CNS.

The transition metal measurements developed in this study have many applications in neurodegenerative diseases in which metal levels have been implicated. With further optimization, the NAA techniques used in this research can be used not only in rodent models, but also in human tissues. We believe that this study can then be extended to human diseases such as multiple sclerosis, where, similarly, the immune-mediated myelin damage needs to be resolved. Understanding the processes in such neurological diseases is of importance to not only elucidating changes in metal levels in disease, but to also design repair promoting therapies.

References

Anderson JG, Fordahl SC, Cooney PT, Weaver TL, Colyer CL, Erikson KM. 2008. Manganese exposure alters extracellular GABA, GABA receptor and transporter protein and mRNA levels in the developing rat brain. Neurotoxicology 29(6):1044-1053.

Aschner M, Erikson KM, Dorman DC. 2005. Manganese dosimetry: Species differences and implications for neurotoxicity. Critical Reviews in Toxicology 35(1):1-32.

Aschner M, Gannon M, Kimelberg HK. 1992. Manganese uptake and efflux in cultured rat astrocytes. Journal of Neurochemistry 58(2):730-735.

Aschner M, Erikson KM, Herrero Hernandez E, Tjalkens R. 2009. Manganese and its role in parkinson's disease: From transport to neuropathology. Neuromolecular Medicine 11(4):252-266.

Badaracco ME, Siri MV, Pasquini JM. 2010. Oligodendrogenesis: The role of iron. BioFactors (Oxford, England) 36(2):98-102.

Beard JL, Connor JR, Jones BC. 1993. Iron in the brain. Nutrition Reviews 51(6):157-170.

Cambron M, D'Haeseleer M, Laureys G, Clinckers R, Debruyne J, De Keyser J. 2012. White-matter astrocytes, axonal energy metabolism, and axonal degeneration in multiple sclerosis. Journal of Cerebral Blood Flow and Metabolism : Official Journal of the International Society of Cerebral Blood Flow and Metabolism 32(3):413-424.

Canavan MM, Cobb S, Drinker CK. 1934. Chronic Manganese Poisoning Report of a Case, with Autopsy. Archives of Neurology & Psychiatry 32(3):501-NP.

Carl GF, Blackwell LK, Barnett FC, Thompson LA, Rissinger CJ, Olin KL, Critchfield JW, Keen CL, Gallagher BB. 1993. Manganese and epilepsy: Brain glutamine synthetase and liver arginase activities in genetically epilepsy prone and chronically seizured rats. Epilepsia 34(3):441-446.

Chen CJ, Ou YC, Lin SY, Liao SL, Chen SY, Chen JH. 2006. Manganese modulates pro-inflammatory gene expression in activated glia. Neurochemistry International 49(1):62-71.

Clark S. 1998. Piranha Etch - The Removal of Organics Using Sulfuric Peroxide. Bold Technologies Inc. Retrieved from: http://www.bold-tech.com/technical/piranha_etch.html

Cole TB, Wenzel HJ, Kafer KE, Schwartzkroin PA, Palmiter RD. 1999. Elimination of zinc from synaptic vesicles in the intact mouse brain by disruption of the ZnT3 gene.

Proceedings of the National Academy of Sciences of the United States of America 96(4):1716-1721.

Connor JR and Menzies SL. 1996. Relationship of iron to oligodendrocytes and myelination. Glia 17(2):83-93.

Connor JR, Menzies SL, St Martin SM, Mufson EJ. 1992. A histochemical study of iron, transferrin, and ferritin in alzheimer's diseased brains. Journal of Neuroscience Research 31(1):75-83.

Corniola RS, Tassabehji NM, Hare J, Sharma G, Levenson CW. 2008. Zinc deficiency impairs neuronal precursor cell proliferation and induces apoptosis via p53-mediated mechanisms. Brain Research 1237:52-61.

De Keyser J, Laureys G, Demol F, Wilczak N, Mostert J, Clinckers R. 2010. Astrocytes as potential targets to suppress inflammatory demyelinating lesions in multiple sclerosis. Neurochemistry International 57(4):446-450.

Delaney K, Kwiecien J, Wegiel J, Wisniewski H, Percy D, Fletch A. 1995. Familial dysmyelination in a long-evans rat mutant. Laboratory Animal Science 45(5):547-553.

Dentinger MP, Barron KD, Csiza CK. 1982. Ultrastructure of the central nervous system in a myelin deficient rat. Journal of Neurocytology 11(4):671-691.

Dietz RM, Weiss JH, Shuttleworth CW. 2008. Zn2+ influx is critical for some forms of spreading depression in brain slices. The Journal of Neuroscience : The Official Journal of the Society for Neuroscience 28(32):8014-8024.

Erikson KM, Dobson AW, Dorman DC, Aschner M. 2004. Manganese exposure and induced oxidative stress in the rat brain. The Science of the Total Environment 334-335:409-416.

Filipov NM and Dodd CA. 2012. Role of glial cells in manganese neurotoxicity. Journal of Applied Toxicology : JAT 32(5):310-317.

Franklin PA, Pullen RG, Hall GH. 1992. Blood-brain exchange routes and distribution of 65Zn in rat brain. Neurochemical Research 17(8):767-771.

Gaasch JA, Lockman PR, Geldenhuys WJ, Allen DD, Van der Schyf CJ. 2007. Brain iron toxicity: Differential responses of astrocytes, neurons, and endothelial cells. Neurochemical Research 32(7):1196-1208.

Garcia SJ, Gellein K, Syversen T, Aschner M. 2006. A manganese-enhanced diet alters brain metals and transporters in the developing rat. Toxicological Sciences : An Official Journal of the Society of Toxicology 92(2):516-525.

Glascock MD. 1988. Tables for neutron activation analysis. Research Reactor Facility, University of Missouri. Columbia, MO. 65211

Goldmann T and Prinz M. 2013. Role of microglia in CNS autoimmunity. Clinical & Developmental Immunology 2013:208093.

Haase H and Rink L. 2009. Functional significance of zinc-related signaling pathways in immune cells. Annual Review of Nutrition 29:133-152.

Hallgren B and Sourander P. 1958. The effect of age on the non-haemin iron in the human brain. Journal of Neurochemistry 3(1):41-51.

Hasan R, Rink L, Haase H. 2013. Zinc signals in neutrophil granulocytes are required for the formation of neutrophil extracellular traps. Innate Immunity 19(3):253-264.

Hu J and Connor JR. 1996. Demonstration and characterization of the iron regulatory protein in human brain. Journal of Neurochemistry 67(2):838-844.

Ishibashi T, Dakin KA, Stevens B, Lee PR, Kozlov SV, Stewart CL, Fields RD. 2006. Astrocytes promote myelination in response to electrical impulses. Neuron 49(6):823-832.

Izawa T, Yamate J, Franklin RJ, Kuwamura M. 2010. Abnormal iron accumulation is involved in the pathogenesis of the demyelinating dmy rat but not in the hypomyelinating mv rat. Brain Research 1349:105-114.

Johansson SV, Plantin LO, Strandberg PO, Uusma K. 1970. Estimation of iron in human bone marrow with histological, chemical and neutron activation analysis. Clinica Chimica Acta; International Journal of Clinical Chemistry 30(3):549-558.

Kahmann L, Uciechowski P, Warmuth S, Plumakers B, Gressner AM, Malavolta M, Mocchegiani E, Rink L. 2008. Zinc supplementation in the elderly reduces spontaneous inflammatory cytokine release and restores T cell functions. Rejuvenation Research 11(1):227-237.

Kawai Y, Aoki I, Umeda M, Higuchi T, Kershaw J, Higuchi M, Silva AC, Tanaka C. 2010. In vivo visualization of reactive gliosis using manganese-enhanced magnetic resonance imaging. NeuroImage 49(4):3122-3131.

Khandaker MU. 2011. High purity germanium detector in gamma-ray spectrometry. International Journal of Fundamental Physical Sciences 1:42-46.

Knoll, G. 2000. Radiation detection and measurement, Third ed. Wiley.

Kozlowski H, Janicka-Klos A, Brasun J, Gaggelli E, Valensin D, Valensin G. 2009. Copper, iron, and zinc ions homeostasis and their role in neurodegenerative

disorders (metal uptake, transport, distribution and regulation). Coordination Chemistry Reviews 253(21):2665-2685.

Kwiecien JM. 2010. Cellular compensatory mechanisms in the CNS of dysmyelinated rats. Comparative Medicine 60(3):205-217.

Kwiecien JM, O'Connor LT, Goetz BD, Delaney KH, Fletch AL, Duncan ID. 1998. Morphological and morphometric studies of the dysmyelinating mutant, the long evans shaker rat. Journal of Neurocytology 27(8):581-591.

Law W, Kelland E, Sharp P, Toms N. 2003. Characterisation of zinc uptake into rat cultured cerebrocortical oligodendrocyte progenitor cells. Neuroscience Letters 352(2):113-116.

Lin DD, Cohen AS, Coulter DA. 2001. Zinc-induced augmentation of excitatory synaptic currents and glutamate receptor responses in hippocampal CA3 neurons. Journal of Neurophysiology 85(3):1185-1196.

Liu M, Cai T, Zhao F, Zheng G, Wang Q, Chen Y, Huang C, Luo W, Chen J. 2009. Effect of microglia activation on dopaminergic neuronal injury induced by manganese, and its possible mechanism. Neurotoxicity Research 16(1):42-49.

Lozoff B and Georgieff MK. 2006. Iron deficiency and brain development. Seminars in Pediatric Neurology 13(3):158-165.

Magaki S, Mueller C, Yellon SM, Fox J, Kim J, Snissarenko E, Chin V, Ghosh MC, Kirsch WM. 2007. Regional dissection and determination of loosely bound and non-heme iron in the developing mouse brain. Brain Research 1158:144-150.

McMaster University. 1996-2013. McMaster Nuclear Reactor: How Does it Work? Hamilton, Ontario. Retrieved from: http://mnr.mcmaster.ca/overview/more-about-mnr.html

Miller RH. 2002. Regulation of oligodendrocyte development in the vertebrate CNS. Progress in Neurobiology 67(6):451-467.

Moldovan N. 2012. Measurement of Transition Metals in the Rodent Brain Using X-ray Fluorescence and Neutron Activation Analysis. McMaster University - Digital Commons.

Moore CS, Abdullah SL, Brown A, Arulpragasam A, Crocker SJ. 2011. How factors secreted from astrocytes impact myelin repair. Journal of Neuroscience Research 89(1):13-21.

Morath DJ and Mayer-Proschel M. 2001. Iron modulates the differentiation of a distinct population of glial precursor cells into oligodendrocytes. Developmental Biology 237(1):232-243.

Morris DR and Levenson CW. 2012. Ion channels and zinc: Mechanisms of neurotoxicity and neurodegeneration. Journal of Toxicology 2012:785647.

Mughabghab S. 2003. Thermal neutron capture cross sections resonance integrals and g-factors. .

Omata N, Murata T, Maruoka N, Ikeda H, Mitsuya H, Mizuno T, Mita K, Asano M, Kiyono Y, Okazawa H, and others. 2012. Effect of dietary zinc deficiency on ischemic vulnerability of the brain. Neuroscience Letters 531(1):10-13.

ORTEC. 2010. Research Applications - Pulse-Height, Charge, or Energy Spectroscopy. Ametek. South Illinois, U.S.A. Retrieved from: http://ortec-online.com/searchresults.aspx?Keywords=pulse-height%20charge%20and%20energy

Pidruczny A, Butler M, Ernst P, Collins M, Avelar J. 1994. The McMaster University Nuclear Reactor (MNR) research facilities. Journal of Radioanalytical and Nuclear Chemistry-Articles 180(2):313-318.

Qian ZM and Wang Q. 1998. Expression of iron transport proteins and excessive iron accumulation in the brain in neurodegenerative disorders. Brain Research.Brain Research Reviews 27(3):257-267.

Quintana C and Gutierrez L. 2010. Could a dysfunction of ferritin be a determinant factor in the aetiology of some neurodegenerative diseases? Biochimica Et Biophysica Acta 1800(8):770-782.

Rama Rao KV, Reddy PV, Hazell AS, Norenberg MD. 2007. Manganese induces cell swelling in cultured astrocytes. Neurotoxicology 28(4):807-812.

Roels H, Lauwerys R, Genet P, Sarhan MJ, de Fays M, Hanotiau I, Buchet JP. 1987. Relationship between external and internal parameters of exposure to manganese in workers from a manganese oxide and salt producing plant. American Journal of Industrial Medicine 11(3):297-305.

Rouault, T.A. and Cooperman, S. 2006. Brain iron metabolism. 13, 142-148.

Sadrzadeh S and Saffari Y. 2004. Iron and brain disorders. American Journal of Clinical Pathology.Pathology Patterns Reviews. 121(Suppl 1):S64.

Sahni V, Leger Y, Panaro L, Allen M, Giffin S, Fury D, Hamm N. 2007. Case report: A metabolic disorder presenting as pediatric manganism. Environmental Health Perspectives 115(12):1776-1779.

Schrag M, Dickson A, Jiffry A, Kirsch D, Vinters HV, Kirsch W. 2010. The effect of formalin fixation on the levels of brain transition metals in archived samples. Biometals : An International Journal on the Role of Metal Ions in Biology, Biochemistry, and Medicine 23(6):1123-1127.

Schulz K, Kroner A, David S. 2012. Iron efflux from astrocytes plays a role in remyelination. The Journal of Neuroscience : The Official Journal of the Society for Neuroscience 32(14):4841-4847.

Schulz K, Vulpe CD, Harris LZ, David S. 2011. Iron efflux from oligodendrocytes is differentially regulated in gray and white matter. The Journal of Neuroscience : The Official Journal of the Society for Neuroscience 31(37):13301-13311.

Shuttleworth CW and Weiss JH. 2011. Zinc: New clues to diverse roles in brain ischemia. Trends in Pharmacological Sciences 32(8):480-486.

Sidoryk-Wegrzynowicz M and Aschner M. 2013a. Manganese toxicity in the central nervous system: The glutamine/glutamate-gamma-aminobutyric acid cycle. Journal of Internal Medicine 273(5):466-477.

Sidoryk-Wegrzynowicz M and Aschner M. 2013b. Role of astrocytes in manganese mediated neurotoxicity. BMC Pharmacology & Toxicology 14:23-6511-14-23.

Skripuletz T, Hackstette D, Bauer K, Gudi V, Pul R, Voss E, Berger K, Kipp M, Baumgartner W, Stangel M. 2013. Astrocytes regulate myelin clearance through recruitment of microglia during cuprizone-induced demyelination. Brain : A Journal of Neurology 136(Pt 1):147-167.

Smith CM, Mayer JA, Duncan ID. 2013. Autophagy promotes oligodendrocyte survival and function following dysmyelination in a long-lived myelin mutant. The Journal of Neuroscience : The Official Journal of the Society for Neuroscience 33(18):8088-8100.

Spranger M, Schwab S, Desiderato S, Bonmann E, Krieger D, Fandrey J. 1998. Manganese augments nitric oxide synthesis in murine astrocytes: A new pathogenetic mechanism in manganism? Experimental Neurology 149(1):277-283.

Szewczyk B. 2013. Zinc homeostasis and neurodegenerative disorders. Frontiers in Aging Neuroscience 5:33.

Tarohda T, Yamamoto M, Amamo R. 2004. Regional distribution of manganese, iron, copper, and zinc in the rat brain during development. Analytical and Bioanalytical Chemistry 380(2):240-246.

University of Missouri. 2008. NAA Quantification. University of Missouri Research Reactor Center. Retrieved from: http://www.murr.missouri.edu/ps_analytical_NAA_quantification.php

University of Missouri. 1996. Overview of X-ray Fluorescence. Archaeometry Laboratory. University of Missouri Research Reactor - Columbia. Retrieved from: http://archaeometry.missouri.edu/xrf_overview.html

University of Utah. 2013. Genetic Science Learning Center - The Other Brain Cells. Salt Lake City, Utah 84108. Retrieved from: http://learn.genetics.utah.edu/content/addiction/reward/cells.html

Wang Y, Me X, Zhang L, Lv G. 2011. Supplement moderate zinc as an effective treatment for spinal cord injury. Medical Hypotheses 77(4):589-590.

Wedler FC and Denman RB. 1984. Glutamine synthetase: The major mn(II) enzyme in mammalian brain. Current Topics in Cellular Regulation 24:153-169.

Williams A, Piaton G, Lubetzki C. 2007. Astrocytes--friends or foes in multiple sclerosis? Glia 55(13):1300-1312.

Yanik M, Kocyigit A, Tutkun H, Vural H, Herken H. 2004. Plasma manganese, selenium, zinc, copper, and iron concentrations in patients with schizophrenia. Biological Trace Element Research 98(2):109-117.

Yokel RA. 2006. Blood-brain barrier flux of aluminum, manganese, iron and other metals suspected to contribute to metal-induced neurodegeneration. Journal of Alzheimer's Disease : JAD 10(2-3):223-253.

Zhang SC, Goetz BD, Carre JL, Duncan ID. 2001. Reactive microglia in dysmyelination and demyelination. Glia 34(2):101-109.

Zhao F, Cai T, Liu M, Zheng G, Luo W, Chen J. 2009. Manganese induces dopaminergic neurodegeneration via microglial activation in a rat model of manganism. Toxicological Sciences : An Official Journal of the Society of Toxicology 107(1):156-164.